The Meteoritical Society

Meteoritics & Planetary Science 46, Nr 9, 1376–1396 (2011)
doi: 10.1111/j.1945-5100.2011.01237.x

Correlated microanalysis of cometary organic grains returned by Stardust

Bradley T. De GREGORIO[1,2*], Rhonda M. STROUD[1], George D. CODY[3], Larry R. NITTLER[4], A. L. DAVID KILCOYNE[5], and Sue WIRICK[6]

[1]Materials Science and Technology Division, Naval Research Laboratory, Washington, District of Columbia, USA
[2]ESCG/NASA Johnson Space Center, Houston, Texas, USA
[3]Geophysical Laboratory, Carnegie Institution of Washington, Washington, District of Columbia, USA
[4]Department of Terrestrial Magnetism, Carnegie Institution of Washington, Washington, District of Columbia, USA
[5]Advanced Light Source, Lawrence Berkeley National Laboratory, Berkeley, California, USA
[6]National Synchrotron Light Source, Brookhaven National Laboratory, Upton, New York, USA
[*]Corresponding author. E-mail: brad.degregorio@gmail.com

(Received 19 March 2011; revision accepted 22 June 2011)

Abstract–Carbonaceous matter in Stardust samples returned from comet 81P/Wild 2 is observed to contain a wide variety of organic functional chemistry. However, some of this chemical variety may be due to contamination or alteration during particle capture in aerogel. We investigated six carbonaceous Stardust samples that had been previously analyzed and six new samples from Stardust Track 80 using correlated transmission electron microscopy (TEM), X-ray absorption near-edge structure spectroscopy (XANES), and secondary ion mass spectroscopy (SIMS). TEM revealed that samples from Track 35 containing abundant aliphatic XANES signatures were predominantly composed of cometary organic matter infilling densified silica aerogel. Aliphatic organic matter from Track 16 was also observed to be soluble in the epoxy embedding medium. The nitrogen-rich samples in this study (from Track 22 and Track 80) both contained metal oxide nanoparticles, and are likely contaminants. Only two types of cometary organic matter appear to be relatively unaltered during particle capture. These are (1) polyaromatic carbonyl-containing organic matter, similar to that observed in insoluble organic matter (IOM) from primitive meteorites, interplanetary dust particles (IDPs), and in other carbonaceous Stardust samples, and (2) highly aromatic refractory organic matter, which primarily constitutes nanoglobule-like features. Anomalous isotopic compositions in some of these samples also confirm their cometary heritage. There also appears to be a significant labile aliphatic component of Wild 2 organic matter, but this material could not be clearly distinguished from carbonaceous contaminants known to be present in the Stardust aerogel collector.

INTRODUCTION

Sample return of cometary dust from comet 81P/Wild 2 by the NASA Stardust mission (Brownlee et al. 2006) potentially enables characterization and analysis of relatively unprocessed organic matter present in the early solar nebula or protosolar molecular cloud. Although primitive organic matter is present in many different extraterrestrial samples, including carbonaceous chondrite meteorites and interplanetary dust particles (IDPs), much of this material has experienced some degree of parent body processing. Anhydrous chondritic-porous IDPs are one potential source of unprocessed primitive organic matter (Messenger 2000; Keller et al. 2004), and are thought to originate in comets (Busemann et al. 2009). The structure of individual comets does vary with time (Stern 2003; Fernández 2008), as demonstrated by flyby imaging of the surfaces of 9P/Tempel 1 (A'Hearn 2005) and 81P/Wild 2 (Brownlee et al. 2004). However, large-scale aqueous and thermal processing of organic matter on comets is minimal and contemporary cometary organic matter should largely reflect the original accreted material.

© The Meteoritical Society, 2011.

Comet Wild 2 accumulated material from both nebular and interstellar sources. Crystalline Mg-rich silicates and CAI-like grains (Zolensky et al. 2006; Ishii et al. 2008), chondrule-like grains (Nakamura et al. 2008), and large noble gas concentrations (Marty et al. 2008) are consistent with formation in the inner solar system, indicating large-scale mixing and radial transport of material to the outer nebula (Brownlee et al. 2006). It is estimated that between one half and two-thirds of the inorganic cometary material has an inner solar system origin (Westphal et al. 2009). The remainder of Wild 2 samples formed in the outer solar system or in interstellar or circumstellar environments represented by presolar grains and organic matter with isotopically anomalous abundances of D and ^{15}N (McKeegan et al. 2006; Matrajt et al. 2008; Stadermann et al. 2008; De Gregorio et al. 2010).

Preliminary examination (PE) of carbonaceous Stardust samples revealed a wide variety of composition and chemical functionality (Keller et al. 2006; Sandford et al. 2006; Cody et al. 2008a; Gallien et al. 2008; Rotundi et al. 2008; Wirick et al. 2009). It is likely that this cometary organic matter contains both volatile and refractory components, as observed in primitive carbonaceous chondrite meteorites (e.g., Alexander et al. 2007; Schmitt-Kopplin et al. 2010). However, due to the nature of the Stardust sample collection, these two distinct classes of organic matter cannot be separated prior to sample analysis. In general, organic matter from Wild 2 is less aromatic than that found in meteorites and IDPs, and it appears to contain proportionately more nitrogen and oxygen (Sandford et al. 2006; Cody et al. 2008a). Nitrogen-rich organics were detected in the dust stream by the cometary and interstellar dust analyzer (CIDA) during the comet flyby (Kissel et al. 2004) and spacecraft collector foils contain enhanced concentrations of cometary methylamine and ethylamine (Glavin et al. 2008) and the simple amino acid glycine (Elsila et al. 2009) on their surfaces. Organic matter is also present in capture tracks in the silica aerogel collectors. Captured polyminerallic terminal particles occasionally contain carbonaceous, rinds, and films (Matrajt et al. 2008; Wirick et al. 2009), while many carbon-rich particles are embedded along the sides of bulbous regions in type II tracks (Cody et al. 2008a; Gallien et al. 2008). Both aromatic (Clemett et al. 2010) and aliphatic (Keller et al. 2006; Rotundi et al. 2008) organics are observed in aerogel tracks and in terminal particles. Organic matter in carbonaceous grains may contain additional diverse chemical functionality, ranging from carboxyl (-COOH), aromatic enol ($C_{arom.}$-OH), and ketone ($C_{arom.}$-C=O) functional groups, which are typical for insoluble organic matter (IOM) in carbonaceous chondrites and IDPs, to organic matter dominated by amide (-$CONH_x$), nitrile (-CN), and alcohol (C-OH) or ether (C-O-C) functional groups (Cody et al. 2008a; Wirick et al. 2009). This diversity of organic functionality is consistent with the unequilibrated nature of the cometary body implied by observations of silicate and sulfide grains in terminal particles (Brownlee et al. 2006).

Such spectroscopic studies of organic functional chemistry are complicated by the possibilities for contaminant particles within the Stardust collection and chemical alteration during the aerogel capture process. Potential contaminants may derive from spacecraft materials, landing site soils, or carbon intrinsic to the aerogel itself (Sandford et al. 2010), although such contaminants have yet to be observed within capture tracks. Hypervelocity impact ($\sim$6 km s^{-1}) into aerogel may heat the captured particles to a peak temperature greater than 1200 °C (Leroux et al. 2008; Rietmeijer et al. 2008), which could vaporize organic matter. However, much evidence exists that suggests that some organic matter can survive hypervelocity impact (Burchell et al. 2006; Noguchi et al. 2007; Spencer et al. 2009; Berger et al. 2011) and that primitive cometary organic matter is present within the capture tracks (Matrajt et al. 2008; Wirick et al. 2009; De Gregorio et al. 2010). Direct imaging of Stardust samples by nano-scale techniques such as transmission electron microscopy (TEM) is essential for distinguishing authentic cometary material from contaminants and/or assessing the degree of alteration due to particle capture.

In this study, we performed TEM on several carbonaceous particles previously characterized by scanning-transmission X-ray microscopy (STXM) as part of the Stardust PE studies (Cody et al. 2008a). The STXM analysis of some PE samples indicated elevated levels of Si or unusual spectral variations, which warranted subsequent nano-scale investigation to rule out contaminants or capture alteration. In addition, we have characterized additional cometary particles from Cometary Track 80 using correlated TEM, STXM, and isotopic analysis by secondary ion mass spectrometry (SIMS).

SAMPLES AND METHODS

Stardust samples analyzed in this study are listed in Table 1. Several ultramicrotomed carbonaceous samples were identified during the Stardust PE (Sandford et al. 2006). They had been extracted from aerogel tracks, epoxy- or sulfur-embedded, and sectioned at the curatorial facility at Johnson Space Center (JSC). Their functional chemistry has been previously characterized by STXM (Cody et al. 2008a). Four new Stardust particles were allocated from Track 80 in cometary aerogel Cell 2092 (Table 1). These particles had been extracted from

Table 1. Stardust samples analyzed in this study.

Sample	Track	Particle	Medium	Thickness (nm)	STXM
FC3,0,2,4,5	2	4	Sulfur	150[a]	ALS 5.3.2
FC9,0,13,1,4	13	1	Sulfur	50[a]	n.a.
FC9,0,13,1,5	13	1	Sulfur	150[a]	#7; #8[b]
FC12,0,16,1,10	16	1	Epoxy	130[a]	#1[b]
C2115,24,22,1,5	22	1	Sulfur	130[a]	#3[b]
C2054,0,35,32,8	35	32	Sulfur	130[a]	#5[b]
C2054,0,35,32,10	35	32	Sulfur	130[a]	#4[b]
C2092,6,80,40,2	80	40	Sulfur	100	ALS 5.3.2
C2092,6,80,40,3	80	40	Sulfur	100	ALS 5.3.2
C2092,6,80,41,1	80	41	Sulfur	200	CLS 10ID-1
C2092,6,80,43,1	80	43	Sulfur	90	NSLS X1A1; ALS 5.3.2
C2092,6,80,43,2	80	43	Sulfur	90	NSLS X1A1; ALS 5.3.2
C2092,6,80,44,2	80	44	Sulfur	100	NSLS X1A1; ALS 5.3.2

Notes: n.a. = not applicable

[a]Section thickness reported in the JSC Stardust catalog.

[b]Numbers refer to sample designations in Cody et al. (2008a). XANES spectra were acquired at ALS. Some discrepancies between the official sample designations between Cody et al. (2008a) and this study are due to typographic errors in the former.

the bulbous region of the type II track by K. Nakamura-Messenger at JSC. Each particle was embedded in molten sulfur using a newly made glass needle. Once the sulfur crystallized around the particle, the solid droplet was attached to a standard epoxy stub with cyanoacrylate adhesive. Samples were ultramicrotomed at a thickness of 90–200 nm and transferred to 200 mesh "slim-bar" Cu TEM grids with a silicon monoxide support film. The sulfur was removed by sublimation in a 60 °C oven for at least 2 h.

Scanning transmission X-ray microscopy analyses were performed at three different synchrotron facilities: beam line X1A1 at the National Synchrotron Light Source (NSLS) at Brookhaven National Laboratory (Winn et al. 2000), beam line 5.3.2 at the Advanced Light Source (ALS) at the Lawrence Berkeley National Laboratory (Kilcoyne et al. 2003), and beam line 10ID-1 at the Canadian Light Source (CLS) at the University of Saskatchewan (Kaznatcheev et al. 2007). Each of these instruments is capable of capturing soft X-ray absorption images with energies between 270 and 340 eV at a spatial resolution of about 25 nm per pixel and an energy resolution of less than 0.1 eV (Winn et al. 2000). The two STXM instruments at ALS and CLS can additionally capture STXM images using X-rays with energies up to 600 eV, allowing full investigation of the C 1*s* (~290 eV), N 1*s* (~410 eV), and O 1*s* (~540 eV) absorption for each sample. Changes in X-ray absorption due to the presence of specific organic functional groups (Table 2) are recorded by first acquiring a series of X-ray absorption images around a particular elemental absorption edge with an energy step as small as 0.1 eV (Jacobsen et al. 2000). After the resulting three-dimensional data sets are spatially aligned by Fourier-transform cross-correlation, each image pixel corresponds to a full X-ray absorption near-edge structure (XANES) spectrum. Clusters of pixels with similar XANES spectral features may either be selected by hand or automatically by principal component analysis and component clustering algorithms (Lerotic et al. 2004). Average transmitted X-ray intensity through the sample at a given energy, $I(E)$, is presented in terms of optical density (OD) relative to the background transmission through the SiO support film, $I_0(E)$, as

$$\mathrm{OD}(E) = -\ln\left[\frac{I(E)}{I_0(E)}\right] \quad (1)$$

This calculation also eliminates contributions from the support film or any amorphous carbon coatings that may have been deposited on the sample and support film. XANES spectra are calibrated against photoabsorptions of CO_2. Tentative identification of functional groups present in organic samples may be confirmed by comparing photoabsorptions in C-XANES, N-XANES, and O-XANES spectra.

All TEM was performed with a JEOL 2200FS 200 keV field-emission microscope at the U.S. Naval Research Laboratory (NRL), equipped with an in-column energy filter and a Noran System Six energy dispersive X-ray spectroscopy (EDS) system. High spatial resolution images were acquired in conventional imaging (TEM) mode or in scanning (STEM) mode using a 0.7 nm probe. Atomic-number contrast STEM images were acquired with a high-angle annular dark-field (HAADF) detector to distinguish carbonaceous matter from denser materials such as metal oxides, silicates, or sulfides. Carbon bonding and organic functionality was observed in some samples by electron energy-loss

Table 2. Characteristic carbon and nitrogen X-ray absorption near-edge structure spectroscopy transition energies.

Functional Group		Transition	Energy (eV)	Reference
Carbon K				
Alkene	C = C	$1s \rightarrow \pi^*$	284.8	(Rightor et al. 1997; Dhez et al. 2003)
Aromatic	C = C	$1s \rightarrow \pi^*$	285.0	(Stöhr 1992)
Imine	C = N	$1s \rightarrow \pi^*$	285.7–285.9	(Dhez et al. 2003; Shard et al. 2004)
Aldehyde	O = CH	$1s \rightarrow \pi^*$	286.3	(Hitchcock and Brion 1980)
Nitrile	C≡N	$1s \rightarrow \pi^*$	286.6–286.7	(Apen et al. 1993; Kikuma et al. 1998; Dhez et al. 2003)
Ketone	C = O	$1s \rightarrow \pi^*$	286.6–286.8	(Hitchcock and Brion 1980; Urquhart and Ade 2002)
Aliphatic	C-C	$1s \rightarrow 3p/s$	287.2–288.3	(Hitchcock and Brion 1980; Ishii and Hitchcock 1988)
Amide	O = C-NH_x	$1s \rightarrow \pi^*$	288.0–288.1	(Urquhart and Ade 2002; Bassim et al. 2008)
Carboxyl	O = C-O	$1s \rightarrow \pi^*$	288.5–288.7	(Urquhart and Ade 2002)
Alcohol, Ether	C-O	$1s \rightarrow 3p/s$	289.0–289.4	(Ishii and Hitchcock 1988)
Urea	$(NH_x)_2CO$	$1s \rightarrow \pi^*$	289.4–289.5	(Urquhart et al. 1995; Urquhart and Ade 2002)
Carbonate	CO_3	$1s \rightarrow \pi^*$	290.3	(Zhou et al. 2008)
Nitrogen K				
Imine	C = N	$1s \rightarrow \pi^*$	398.8	(Apen et al. 1993; Leinweber et al. 2007)
Nitrile	C≡N	$1s \rightarrow \pi^*$	399.7–399.9	(Shard et al. 2004; Leinweber et al. 2007)
Amide	O = C-NH_x	$1s \rightarrow \pi^*$	401.4–401.5	(Gordon et al. 2003; Leinweber et al. 2007)
Urea	$(NH_x)_2CO$	$1s \rightarrow 3p/s$	401.5–401.7	(Urquhart et al. 1995)
Pyrrole	C_4H_4NH	$1s \rightarrow \pi^*$	402.2–402.4	(Leinweber et al. 2007)

spectroscopy (EELS), with a spectral resolution of 0.8–1.1 eV, as defined by the full-width at half-maximum of the zero energy-loss peak. Unfortunately, this energy resolution is almost an order of magnitude worse than that in corresponding XANES spectra, and many photoabsorption peaks in XANES spectra could not be adequately resolved in EELS spectra.

Many carbonaceous sections analyzed during the Stardust PE contained evidence for predominantly aliphatic organic matter (Cody et al. 2008a; Rotundi et al. 2008). As volatile and aliphatic organics may be severely damaged and altered by exposure to a high energy electron beam, TEM analysis was, in most cases, performed only after STXM analysis. Unfortunately, any volatile organics present would also likely be damaged by the STXM beam (Wirick et al. 2009). Therefore, this combination of analytical techniques will not likely allow the observation of unprotected volatile organic matter in Stardust samples. However, less volatile organics may still be present within refractory material or mixed with associated mineral grains or aerogel. To mitigate charging effects from the insulating SiO support film, a thin coating of amorphous carbon was added to the underside of the TEM grids prior to TEM observation. Minor contributions from this carbon coat appear in EDS and EELS spectra, but may be removed from XANES spectra by proper background subtraction, as described above. The only other potential candidate for contamination from sample preparation is the cyanoacrylate adhesive used to attach the sulfur droplet to the epoxy stub. Fortunately, cyanoacrylate exhibits characteristic XANES and EELS spectral features and may be identified unambiguously.

Secondary ion mass spectroscopy was performed on some samples after TEM and STXM analysis to measure their carbon and nitrogen isotopic composition. All measurements were performed in imaging mode with a Cameca NanoSIMS 50L ion microprobe in the Department of Terrestrial Magnetism at the Carnegie Institution of Washington. TEM grids were first attached to 1 cm Al stub mounts with colloidal Ag paint and then coated with Au to eliminate charging effects. A Cs^+ beam with a nominal diameter of 100 nm was rastered over samples and negatively charged secondary ions were collected in multicollection mode along with secondary electrons. Cyanide ions ($^{12}C^{14}N^-$ and $^{12}C^{15}N^-$) were measured as proxies for the nitrogen isotopes. In some samples, carbon and/or nitrogen isotope ratios were not measured, either due to low abundance or artificial contributions from surrounding epoxy and/or carbon support film. Isotope images were analyzed quantitatively with the L'image software (L. Nittler, CIW). Well-characterized IOM from the carbonaceous chondrites Grosvenor Mountains 95577 and Queen Elizabeth Range 99177 (Alexander et al. 2007) was used to calibrate the instrumental fractionation for carbon and nitrogen isotopic ratios and the relative sensitivity factor used to convert measured CN^-/C^- ratios to atomic N/C ratios. Within the uncertainties of the SIMS measurements, these IOM standards should be appropriate for both refractory and volatile organic matter that may be present in the Stardust samples. The ultramicrotomed

samples were, for all practical purposes, consumed during the NanoSIMS analyses.

RESULTS

Preliminary Examination Samples

Track 35

Previous STXM imaging of carbonaceous Stardust PE samples suggested that the particles were composed primarily of organic matter with some contribution from inorganic materials, predominantly silica aerogel (Cody et al. 2008a). The presence of aerogel in these ultramicrotomed sections was inferred from the reduced intensity of the ionization edge of C 1*s* electrons relative to pre-edge background absorption, which may be used to estimate the atomic Si/C ratio from tabulated mass absorption coefficients for each element (Henke et al. 1993). However, identification and characterization of silica aerogel is relatively straightforward with TEM (Stroud et al. 2004). This is exemplified by two adjacent sections from Track 35, Particle 32 (C2054,0,35,32,8 and C2054,0,35,32,10), for which previous STXM data indicated elevated levels of silica associated with organic matter (Cody et al. 2008a). In particular, these data suggested that sample C2054,0,35,32,8 contained two compositionally distinct regions—an inner "band" with increased atomic N/C and O/C surrounded by a lobate region with relatively lower N/C and O/C ratios. Subsequent TEM analysis reveals that both Track 35 samples contain abundant densified aerogel, characterized by a collapsed network of silica mesoparticles (Stroud et al. 2004), and are intermixed with organic matter (Fig. 1). According to hyperspectral EDS maps and spot analyses, the inner band of sample C2054,0,35,32,8 is relatively free of aerogel but consists of a nano-scale aggregate of mineral material with interstitial organic matter (Figs. 1C and 1D). This polymineralic band contains significant iron, magnesium, nickel, and sulfur, in the form of metal sulfides and silicates. Unfortunately, the band region is too thick for high-resolution imaging and electron diffraction necessary to identify the particular minerals present in the band. The presence of sharp, well-defined mineral boundaries in STEM and HAADF images suggest that the sample has not been melted during particle capture.

In both samples from Track 35, Particle 32, the organic matter infiltrating the silica aerogel is dominantly aliphatic, consisting of hydrocarbon chains, with smaller amounts of aromatic ring structures and various carbonyl function groups (Cody et al. 2008a). These results are confirmed by the detection of abundant aliphatic material in this particle by Raman spectroscopy (Rotundi et al. 2008). TEM images of the aerogel in these sections show a reduction of microporosity and an increase in mesoparticle size (densification) from particle capture (Fig. 1E). The observed aerogel texture indicates a combination of densification through both compression and thermal sintering (Phalippou et al. 2004). The remaining pore space is filled by organic matter, obscuring the edges of pores in TEM images. It is possible that this intimate mixture of organic matter and densified aerogel could be the source of past difficulties of interpreting in situ spectroscopic data from other carbon-containing particles from this track (Muñoz Caro et al. 2008).

Nitrogen isotopes were measured in sample C2054,0,35,32,8 and found to be isotopically normal within the measurement uncertainty (Table 3) and homogenously distributed on a μm scale. Unfortunately, the primary ion beam of the NanoSIMS was inadvertently defocused for the measurement, precluding any determination of sub-μm isotopic heterogeneity.

Track 13

Other carbonaceous samples analyzed by STXM during the Stardust PE appeared to be relatively free of silica, exhibiting low Si/C values (Cody et al. 2008a). Ultramicrotome slices from the terminal particle of Track 13 were analyzed by a number of analytical techniques. Raman spectroscopy of one slice indicated a highly disordered carbonaceous material (Sandford et al. 2006; Rotundi et al. 2008), while a SIMS measurement of the same slice revealed it to be enriched in deuterium ($\delta D = 900‰$), confirming its extraterrestrial origin (McKeegan et al. 2006). TEM images of two adjacent ultramicrotome slices from the Track 13 particle (FC9,0,13,1,5) are shown in Fig. 2. They are composed primarily of dense carbonaceous matter and contain lobate morphological features. Both sections are roughly equiform, with the second section (Fig. 2B) having rolled edges from the ultramicrotomy procedure. Previous STXM analysis of these sections indicated the organic matter contained aromatic carbon, aromatic ketone, and carboxyl functional groups (Fig. 7B; Sandford et al. 2006; Cody et al. 2008a). These are the same chemical functionalities observed in most IOM from meteorites and IDPs, although the abundance of aromatic carbon is relatively depleted in the Stardust samples. We found further evidence of carboxyl functional groups in EELS spectra of both sections from Track 13 as small energy-loss peaks around 288 eV (Figs. 3B, 3C, and 3D). An adjacent ultramicrotome slice from the Track 13 particle (FC9,0,13,1,4) contains no carbonaceous matter, but rather consists of a single enstatite grain ($En_{92}Fs_8$; Fig. 2C). Subsequent oxygen isotopic analysis of this grain indicated a nebular origin (Messenger et al. 2008a).

NanoSIMS analysis of FC9,0,13,1,5 revealed a small ^{15}N enrichment ($\delta^{15}N = 70 \pm 22‰$; Table 3) in one of

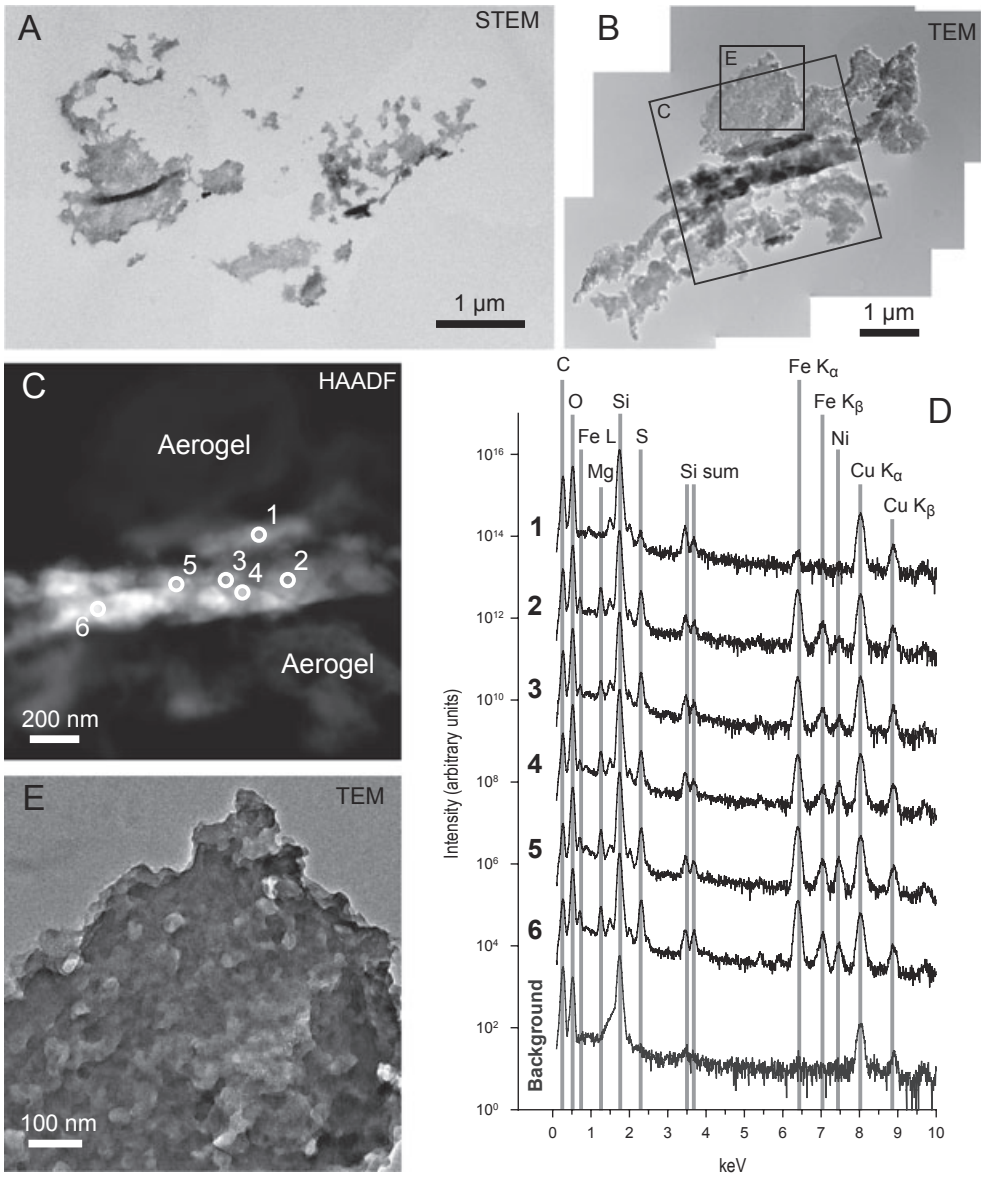

Fig. 1. Transmission electron microscopy (TEM) and scanning transmission electron microscopy (STEM) of ultramicrotomed carbonaceous particles from Stardust Track 35. Samples (A) C2054,0,35,32,10 and (B) C2054,0,35,32,8 contain densified silica aerogel infiltrated by cometary organic matter. (C) High-angle annular dark-field image of the minerallic "band" region of C2054,0,35,32,8 containing nanoscale cometary crystalline material, surrounded by aerogel. (D) Energy dispersive X-ray spectroscopy (EDS) analyses of sulfide and silicate materials within the band region, plotted on a logarithmic scale to show the presence of less abundant elements. Spectrum 1 is representative of silica aerogel mixed with organic matter. Although the central band contains a similar overall abundance of C as that in the surrounding aerogel, it appears depleted in these EDS spectra because of the predominance of inorganic grains. (E) Bright-field TEM image of compressed silica aerogel containing organic matter.

the two ultramicrotome sections (Fig. 2B), providing additional evidence that this particle is a genuine cometary sample. However, the N isotopic composition measured in the other section was normal. A similar isotopic heterogeneity in D/H was observed previously for this particle (McKeegan et al. 2006), suggesting that organic matter in comet Wild 2 is isotopically heterogeneous on sub-μm scales, as observed in carbonaceous matter in primitive meteorites and IDPs (Messenger 2000; Busemann et al. 2006). The average atomic N/C ratio determined by NanoSIMS for the two sections is 0.1, in good agreement with the value of 0.095 determined by STXM (Cody et al. 2008a).

Track 22

Two additional carbonaceous sections from the terminal particle of Track 22 also do not contain any evidence of silica aerogel (Fig. 4). In TEM images, both of

Table 3. Isotopic and elemental compositions of Stardust samples.

Sample	$\delta^{13}C$ (‰)	$\delta^{15}N$ (‰)	N/C (XANES)	N/C (SIMS)	O/C (XANES)
FC3,0,2,4,5[a]	−35 ± 3	−7 ± 5	n.m.	0.08–0.16	n.m.
FC9,0,13,1,5 (Fig. 2A)	−23 ± 19	−27 ± 34	0.07 ± 0.01[b]	0.028	0.19 ± 0.01[b]
FC9,0,13,1,5 (Fig. 2B)	−56 ± 22	70 ± 22	0.12 ± 0.01[b]	0.18	0.22 ± 0.01[b]
FC12,0,16,1,10	n.m.	10 ± 3	0.12[b]	n.m.	0.59 ± 0.05[b]
C2115,24,22,1,5	n.m.	n.m.	0.24 ± 0.03[b]	n.m.	0.18 ± 0.02[b]
C2054,0,35,32,8	n.m.	−55 ± 61	0.12 ± 0.01[b]	n.m.	0.28 ± 0.03[b]
C2054,0,35,32,10	n.m.	n.m.	0.07 ± 0.02[b]	n.m.	0.25 ± 0.03[b]
C2092,6,80,41,1	n.m.	n.m.	0.03 ± 0.02	< 0.002	0.02 ± 0.02
C2092,6,80,43,2A[a] (Fig. 6A)	−42 ± 14	136 ± 15	n.m.	0.10–0.15	n.m.
C2092,6,80,43,2B (Fig. 6B)	−33 ± 10	15 ± 11	0.36 ± 0.06	0.20	0.43 ± 0.05

Notes: n.m. = not measured
[a]Previously reported in De Gregorio et al. (2010).
[b]Previously reported in Cody et al. (2008a).

these sections contain dense, refractory organic matter with sharp edges. The larger of the sections contains 100 nm vesicular features and a 1.6 μm linear feature that appears to be composed of aggregated voids or bubbles. Previous STXM analysis of these sections indicated N-rich functionality (atomic N/C = 0.24) dominated by amide (-$CONH_x$) bonding, with only a small contribution from aromatic carbon bonding (Cody et al. 2008a). This functional chemistry and composition is similar to polymers such as polyacrylamide or nylon, but as these materials were not used on the Stardust spacecraft and XANES studies of possible contaminants (Sandford et al. 2010) do not generate similar spectra as that of the Track 22 sections, the provenance of the Track 22 sections is unclear. However, TEM reveals that the smaller of the two sections contains several 150 nm crystalline grains with a large atomic mass relative to the organic matter (Fig. 4B). EDS analysis indicates that Ti is the only additional element present, along with an average increase in the intensity of the O K_α peak (Fig. 4C). High-resolution TEM imaging of one of these Ti-rich crystallites reveals the presence of 3.47 Å lattice fringes (Fig. 4D). Metallic Ti and rutile (TiO_2) do not have compatible lattice spacings, but plane spacings for the common TiO_2 polymorphs anatase (3.52 Å for (011) reflections) and brookite (3.47 Å for (111) and 3.51 Å for (120) reflections) are similar. An electron diffraction pattern of the Ti-rich crystallite matches the [311] zone axis of anatase (Fig. 4E), which includes the (011) reflections seen in the corresponding high-resolution image. The polymeric nature of the organic matter and the presence of TiO_2 crystallites suggest that this particular sample is most likely an unexpected contaminant.

Energy dispersive X-ray spectroscopy analysis of the polymeric sections from the Track 22 particle also indicates the presence of abundant sulfur in addition to nitrogen (Fig. 4C). While it is possible that the sulfur in these sections is due to infiltration of molten material during sulfur embedding, significant sulfur EDS peaks are not observed in other sulfur-embedded particles, so it is likely that the sulfur in these N-rich sections is authigenic.

Track 16

One of the Stardust PE samples from Track 16 (FC12,0,16,1,10) is a terminal particle that was embedded and ultramicrotomed in epoxy rather than in sulfur. Interestingly, an organic phase with slightly different X-ray absorption properties than epoxy was observed surrounding the terminal particle (Cody et al. 2008a). XANES analysis indicated that this organic phase had similar structure and bonding to the surrounding epoxy with about 10% contribution from a soluble aliphatic component. This epoxy-organic mixture is clearly visible in TEM and STEM images, indicating that it has a lower density than the surrounding epoxy (Fig. 5). It also contains rounded and irregularly shaped void spaces suggesting the degassing of volatiles as the epoxy hardened around it. EELS spectra of both the porous epoxy-organic mixture and the surrounding epoxy appear similar (Fig. 3E). Evidence for chlorine is present in EDS spectra of epoxy but is absent in spot analyses of the epoxy-organic mixture (Fig. 7C). Unfortunately, the Cl abundance in the epoxy was not large enough to perform reliable Cl-based hyperspectral mapping of the epoxy-organic mixture within the section. In addition, the sample contains isotopically normal N (Table 3), but this isotopic composition is likely dominated by epoxy.

Track 80 Samples

Correlated STXM and TEM characterization of new particles from Stardust Track 80 reveal wide variations in morphology and functional chemistry of carbonaceous sections. Sample C2092,6,80,43,2, which contains two

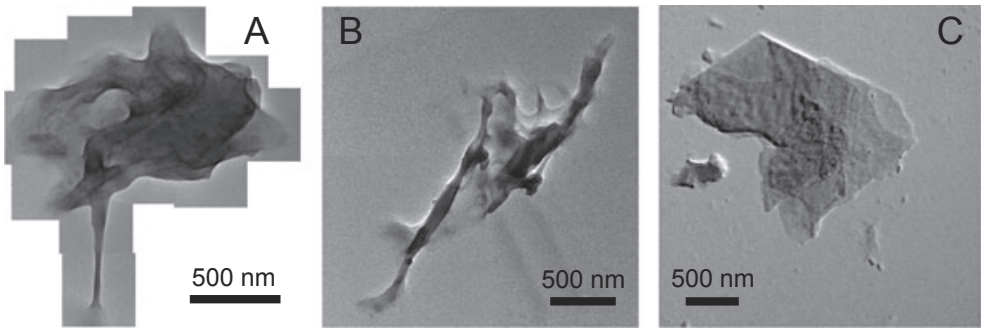

Fig. 2. (A, B) Transmission electron microscopy (TEM) images of two adjacent ultramicrotomed sections from FC9,0,13,1,5 containing dense, lobate, organic matter. (C) A different section of the same particle (FC9,0,13,1,4) only consisted of a single enstatite grain ($En_{92}Fs_8$) with no associated carbonaceous matter.

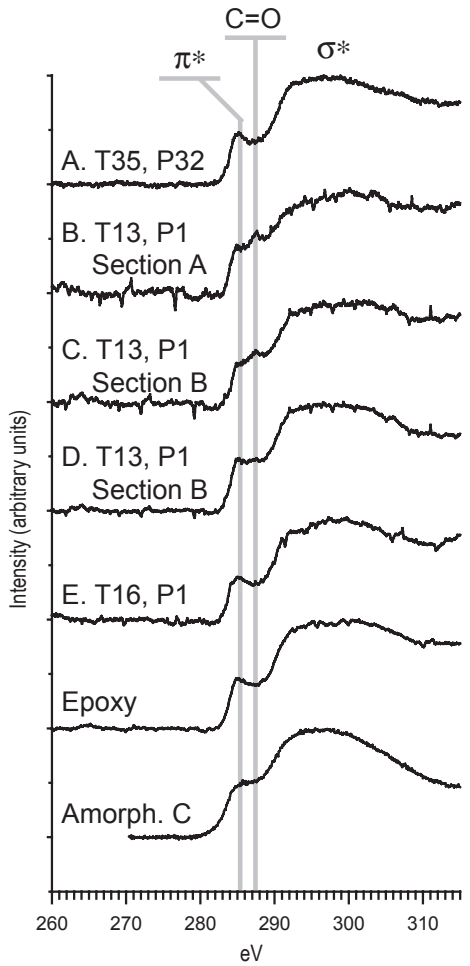

Fig. 3. Electron energy loss spectroscopy (EELS) spectra of organic matter from the Stardust Preliminary Examination. (A) Organic matter in compressed aerogel from sample C2054,0,35,32,10 (Fig. 1A). (B, C, D) Solitary organic matter in sample FC9,0,13,1,5. Spectrum B was acquired from the organic matter shown in Fig. 2A, while Spectra C and D were acquired from the organic matter shown in Fig. 2B. (E) Epoxy and organic mixture from sample FC12,0,16,1,10. (F) Pure epoxy in sample FC12,0,16,1,10. (G) Laboratory-produced amorphous carbon film.

distinct ultramicrotomed sections, exemplifies this diversity. The first, designated informally herein as Section A (Fig. 6A), represents an early slice near the edge of Particle 43, while the other, designated as Section B (Fig. 6B), is a roughly circular slice through the center of Particle 43 with a 5 μm diameter. Section A contains compressed silica aerogel at both ends, while the center contains mostly refractory organic matter. However, carbon analyses by EDS, XANES, EELS, and NanoSIMS indicate that organic matter is present throughout the entire section and infiltrates the silica aerogel as well. Although both sections appear to be nearby microtome slices of the same particle, the functionality and organic bonding in each section are distinct.

The functional group distribution and isotopic composition of Section A were previously described by De Gregorio et al. (2010) in relation to an organic globule (Fig. 6C), similar to those observed in primitive carbonaceous meteorites (Garvie and Buseck 2004; Nakamura-Messenger et al. 2006), associated with the section. The XANES spectrum of this section (Fig. 7A) contain photoabsorptions due to aromatic carbon-carbon bonding, aromatic ketones, and carboxyl functional groups (Table 2), similar to XANES spectra from the organic matter from Track 13 (Fig. 7B, and Spectra 7 and 8 from Fig. 1 of Cody et al. 2008a). These spectra imply that the cometary organic matter in this particle consists of complex polyaromatic domains modified by oxygenic functional groups and interconnected by short aliphatic chains (Cody et al. 2008a; De Gregorio et al. 2010).

In contrast, the XANES spectrum of adjacent Section B (Fig. 7C) is dominated by a large peak centered around 286.6 eV. While this peak could be interpreted to arise from the presence of abundant aromatic ketones, as is the case for Section A, it could also be due to the presence of organic nitriles (C≡N; Table 2). On the lower energy side of this 286.6 eV peak lies a "shoulder" centered around 285 eV due to the

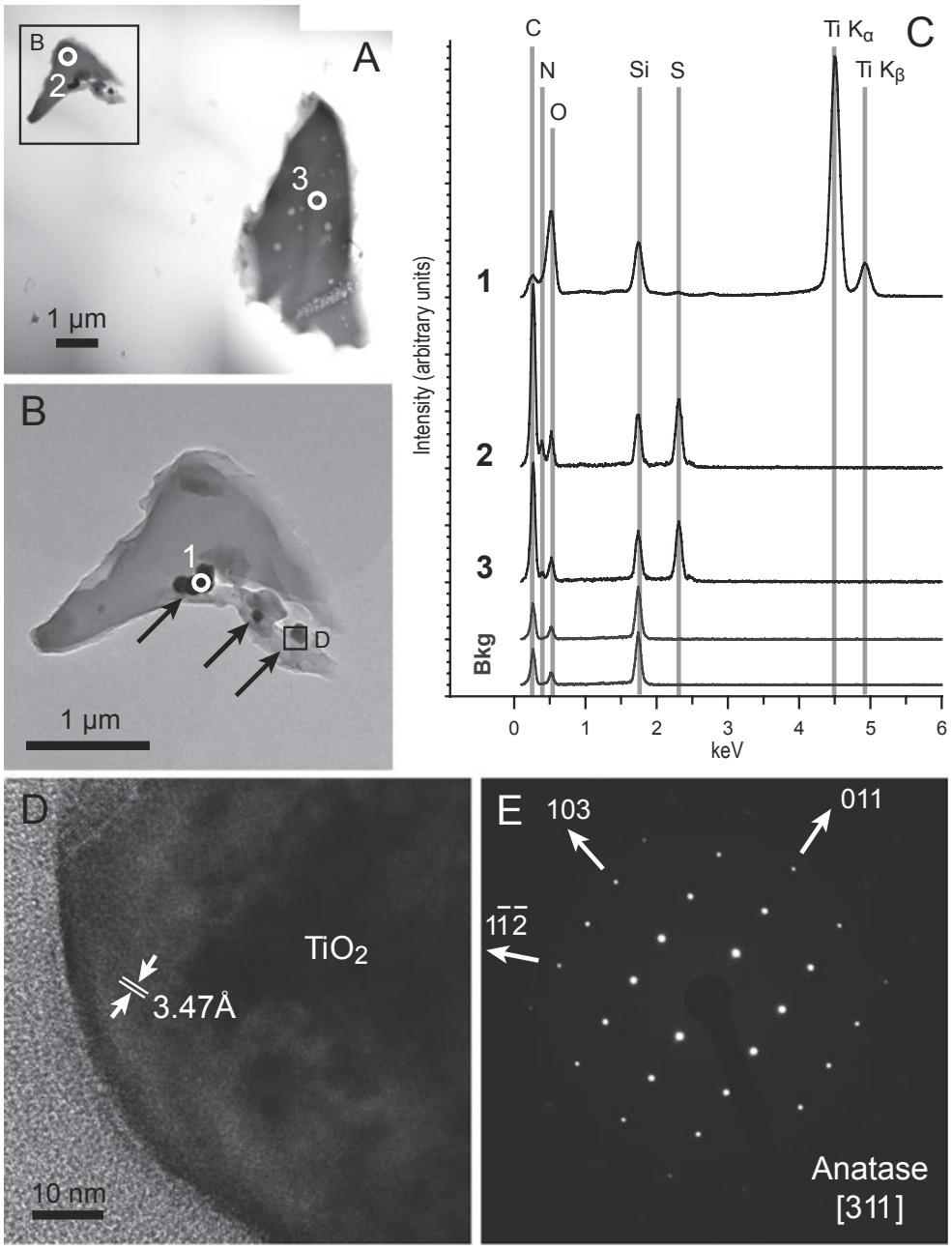

Fig. 4. Transmission electron microscopy (TEM) of ultramicrotomed carbonaceous particles in Stardust sample C2115,24,22,1,5. (A) TEM image mosaic of both sections and (B) a higher resolution image of the smaller organic section containing Ti-rich crystallites (arrows). (C) Energy dispersive X-ray spectroscopy (EDS) analysis of the sample. Spectrum 1 was acquired from the Ti-rich crystallites in (B), while the locations of Spectra 2 and 3 are shown in (A) compared with the background contribution from the carbon-coated SiO support film (Bkg). (D) High-resolution TEM image of a TiO_2 crystallite showing 3.47 Å lattice spacings. (E) Electron diffraction pattern of the same region consistent with the crystal structure of anatase.

presence of aromatic carbon-carbon bonding. Unlike the previous organic section from this particle, there is no clear photoabsorption at 288.5 eV from carboxyl (COOH) functional groups. Rather, the distinct photoabsorption in this spectrum at 288.0 eV may be due the presence of functionally similar amine ($CONH_x$) groups (Table 2). This alternative interpretation is supported by the presence of distinct photoabsorptions from imine (C = N), nitrile (C≡N), and amine ($CONH_x$) functional groups at the N K-edge (Fig. 8A). In fact, the photoabsorption increase above the N ionization energy (~410 eV) observed in the N-XANES spectrum indicates

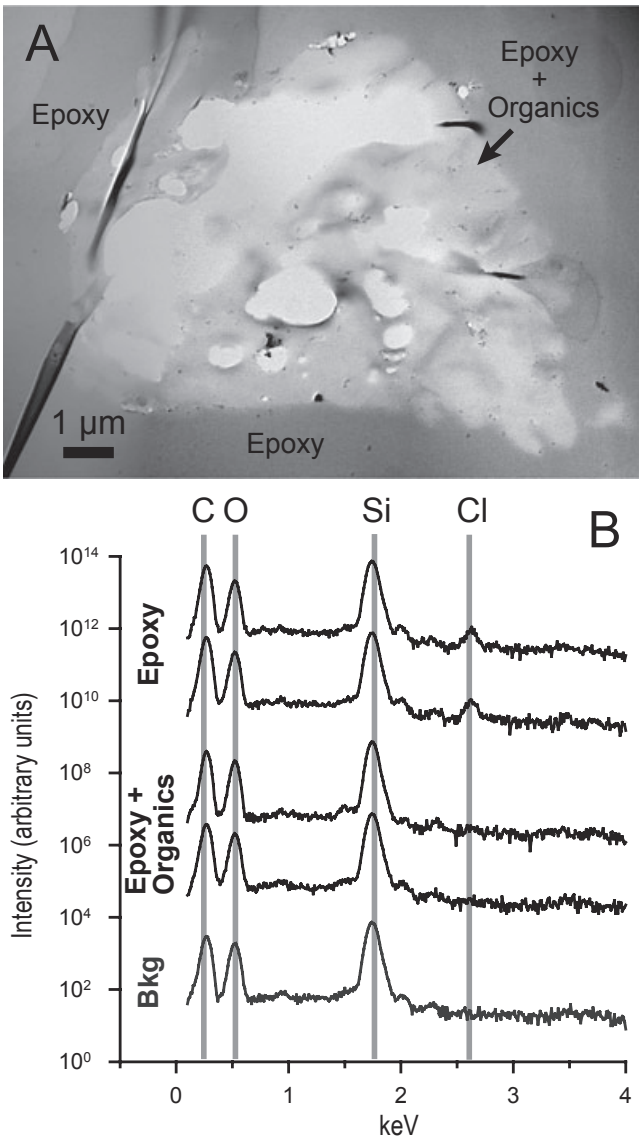

Fig. 5. (A) Bright-field scanning transmission electron microscopy (STEM) image of epoxy-soluble organic matter in sample FC12,0,16,1,10. (B) EDS analyses of the surrounding epoxy and the epoxy-soluble organic matter, plotted on a logarithmic scale to show the presence of trace amounts of chlorine and compared with the background contribution from the carbon-coated SiO support film (Bkg).

that this section is extremely N-rich. Using the method outlined in Cody et al. (2008a) for estimating elemental abundances by modeling C-, N-, and O-XANES spectra with mass absorption coefficients, the organic matter in Section B has an atomic N/C = 0.36 ± 0.06 and O/C = 0.43 ± 0.05. From these elemental ratios, this section represents the most N-rich organic matter found in the Stardust collection.

Both of these sections contain nanoparticles with a higher mass-density than the surrounding organic matter and aerogel and appear as bright spots in HAADF images. Although these nanoparticles are too small for robust mineral identification from electron diffraction patterns, EDS spot analyses indicate the presence of Fe-, Al-, Ti-, Si-, Cr-, and Zr-oxides and/or native metals (Fig. 6D and 6E). Three Fe-free Cr-rich nanoparticles (at least one of which is a Cr metal grain) and an (Fe, Ni)-rich metal grain are all located in Section A (Spectrum 1 in Fig. 6E), while a Zr-oxide nanoparticle, possibly baddeleyite (ZrO_2), is located in Section B (Spectrum 7 in Fig. 6E). The remainder of the metal oxide nanoparticles is located in the N-rich Section B, in addition to a ~100 nm cluster of turbostratic carbon.

Additional ultramicrotomed sections from Particle 43 (C2092,6,80,43,1) contain several 1–4 μm organic-rich grains surrounded by a thin organic residue, likely small amounts of cyanoacrylate adhesive that had penetrated into fine fractures in the crystallized sulfur bead. These grains contain various mineralogies, including a Ca-carbonate and a possible carbonate-fluorapatite, based on correlated XANES and EDS data. However, these grains are likely contaminant particles introduced during the embedding or ultramicrotomy process. No associated aerogel was found with these grains, and the ultramicrotome sections on this TEM grid were collected prior to the sample C2092,6,80,43,2, which contained the cometary organic matter and associated aerogel described in the previous paragraphs. Thus, the sectioned grains in C2092,6,80,43,1 were sampled closer to the surface of the sulfur bead, where the likelihood of addition of terrestrial, organic-rich dust is relatively high.

Another particle (Particle 41) from Track 80 (C2092,6,80,41,1) consists of a single 1 μm spherical, refractory organic grain (Fig. 9). XANES spectra collected from this particle were distinct from those of the two different organics observed in Particle 43 (Fig. 7E). Organic matter in Particle 41 is dominated by aromatic carbon-carbon bonding with little intensity due to carbon-oxygen functional groups observed in the sections from Particle 43. The broad aromatic peak in the XANES spectrum from Particle 41 can be most accurately modeled by two Gaussian photoabsorption peaks centered at 284.7 and 286.2 eV. The former energy indicates the presence of abundant aliphatic C=C bonds in addition to aromatic C=C in polyaromatic domains. The latter energy is slightly higher than the photoabsorption energy expected of heterocyclic imines (C=N) but is similar to that expected for aldehyde (-CHO) functional groups (Table 2). Cody et al. (2008a) interpret photoabsorptions between 286.1 and 286.3 to be due to aryl ketone, or carbonyl groups (C=O) attached to aromatic rings. This suggests that the majority of the O atoms in this sample are present in carbonyl-type functional groups modifying polyaromatic

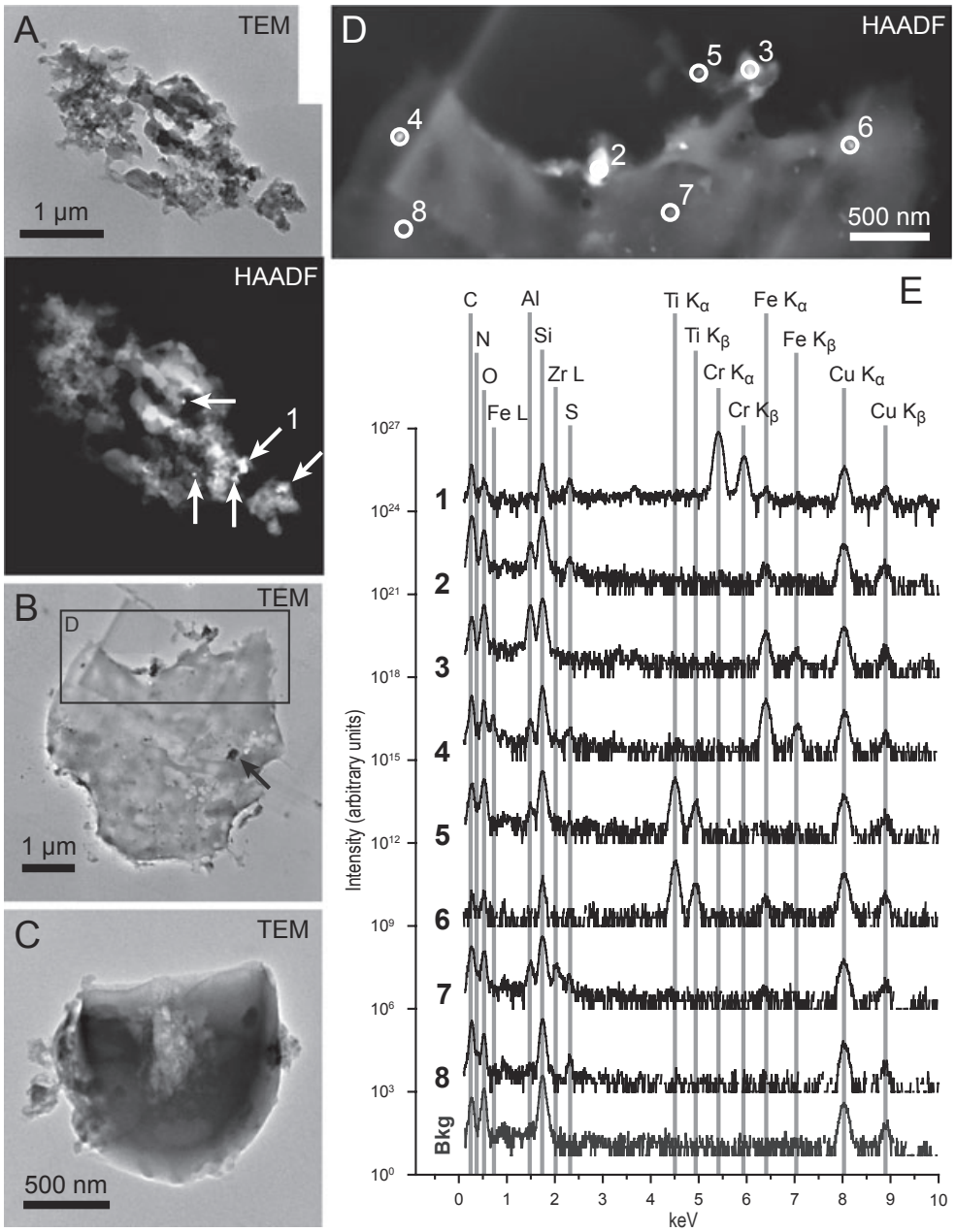

Fig. 6. Transmission electron microscopy (TEM) and scanning transmission electron microscopy (STEM) of ultramicrotomed carbonaceous particles from Stardust Track 80, Particle 43 (C2092,6,80,43,2). (A) Bright-field TEM and High-angle annular dark-field (HAADF) images of cometary organics capped by compressed silica aerogel containing several nanoparticles (arrows). (B) Aerogel-free organic matter containing abundant nanoparticles (arrow denotes location of ~100 nm particle of turbostratic carbon). (C) A cometary organic globule, previously described in De Gregorio et al. (2010). (D) HAADF image of high-atomic mass nanoparticles embedded in carbonaceous matter. (E) EDS analyses of some nanoparticles containing C, Si, Al, Fe, Ti, and Zr plotted on a logarithmic scale to show the presence of less abundant elements, compared with the background contribution from the carbon-coated SiO support film (Bkg). Spectrum 7 also contains a Zr K peak at 15.7 keV. Spectrum 8 samples the N-rich carbonaceous matter comprising the bulk particle.

domains. N- and O-XANES spectra of the organic matter indicate the presence of relatively little N and O, with atomic N/C = 0.03 ± 0.02 and O/C = 0.02 ± 0.02. This low N abundance made it impossible to measure an accurate $^{14}N/^{15}N$ ratio by SIMS.

Ultramicrotomed sections from Particles 40 and 44 of Track 80 contained only compressed and melted aerogel. These sections were similar to others recovered from the ''bulb'' region of Track 80, described by Stodolna et al. (2009).

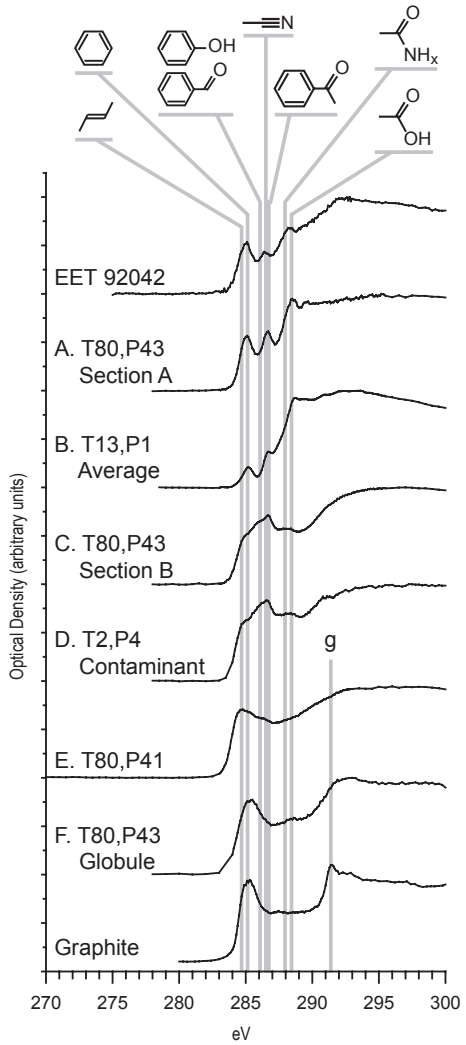

Fig. 7. Carbon-X-ray absorption near-edge structure spectroscopy (C-XANES) spectra of (A) sample C2092,6,80,43,2A (Fig. 6A), (B) an average of adjacent organic ultramicrotome sections from sample FC9,0,13,1,5 (modified from Cody et al. 2008a), (C) sample C2092,6,80,43,2B (Fig. 6B), (D) a possible organic contaminant from sample FC3,0,2,4,5 (De Gregorio et al. 2010), (E) sample C2092,6,80,41,1, and (F) a cometary organic globule from sample C2092,6,80,43,2 (De Gregorio et al. 2010), compared with spectra of graphite and IOM from the primitive meteorite EET 92042. The position of the characteristic graphite exciton photoabsorption is denoted by "g."

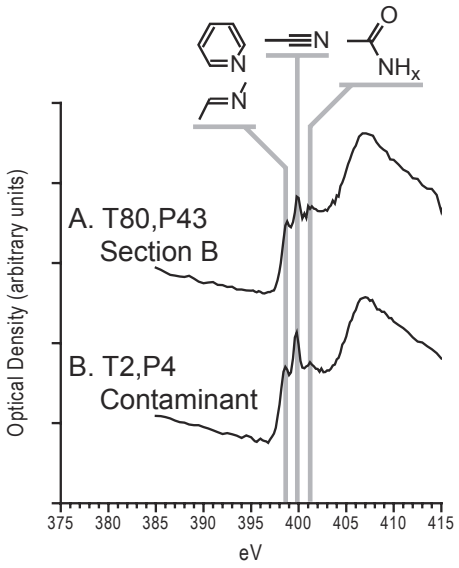

Fig. 8. N-X-ray absorption near-edge structure spectroscopy (N-XANES) spectra of (A) sample C2092,6,80,43,2B (Fig. 1G) and (B) a probable organic contaminant from sample FC3,0,2,4,5 (De Gregorio et al. 2010). Data were collected at beamline 5.3.2 at the Advanced Light Source.

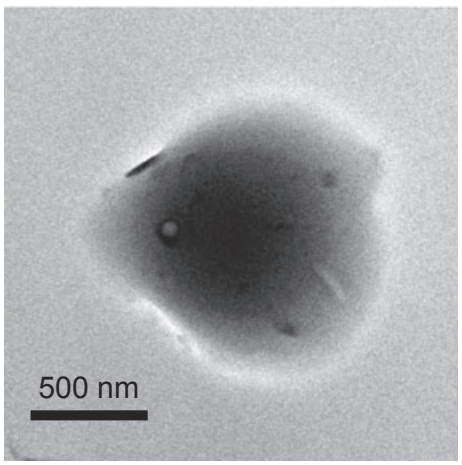

Fig. 9. Transmission electron microscopy (TEM) image of Particle 41 from Track 80 (C2092,6,80,41,1), which may possibly represent a cometary organic globule. A 500 nm circular TEM-induced damage region is visible in the center of the particle from EDS spot analysis.

DISCUSSION

Interaction of Cometary Organic Matter with Aerogel

To accurately characterize carbonaceous matter present in its natural state within comet Wild 2, our analyses and observations of organic samples from the Stardust collection must first be calibrated to identify the effects of particle capture, sample preparation, and organic contamination, both intrinsic to the aerogel capture medium and that introduced later. Perhaps the most controversial of these is the survival and alteration of cometary organic matter during aerogel capture. Cometary dust from Wild 2 impacted the Stardust collector array at a velocity of 6.1 km s^{-1} and was brought to rest after several mm by aerogel compression (Dominguez et al. 2004). Frictional heating during this process may heat the captured particle and surrounding aerogel to temperatures in excess of 1200 °C, causing

melting of mineral grains and silica aerogel (Leroux et al. 2008; Rietmeijer et al. 2008). Gas-gun test shots using coated polystyrene grains showed significant ablation and mass loss during aerogel capture (Burchell et al. 2009). Any captured cometary organic matter could be destroyed under these conditions. However, extreme temperature gradients as large as 2500 °C μm^{-1} may exist, preserving material in the interior of captured particles (Noguchi et al. 2007). Cometary aggregate particles may enhance this effect by combining materials with varied thermal conductivity. The bulk of several different carbonaceous samples was unaltered during light-gas gun shots of 50 μm particles into silica aerogel (Spencer et al. 2009). A cubanite ($CuFe_2S_3$) grain discovered in a terminal particle indicates that the exterior surface temperature of the captured particle never exceeded 210 °C (Berger et al. 2011), and light-gas gun test shots of several mineral particles also suggest that many of these captured grains did not experience temperatures above 200 °C (Burchell et al. 2006). Thermal experiments on meteoritic IOM, which may be structurally and chemically similar to refractory cometary organic matter, found that IOM survives extended exposure to high temperatures (Cody et al. 2008b). Several studies have indicated that aerogel capture is largely reducing (Marcus et al. 2008; Leroux et al. 2009; Wozniakiewicz et al. 2010), such that organic matter would not be additionally altered or destroyed by oxidative reactions. It is then possible that relatively unaltered cometary organic matter may survive aerogel capture, especially if it is present in the interiors of intact particles.

Volatile cometary organic matter would likely have responded differently during the capture process than the more refractory organic matter discussed above. Only a small portion of the total volatile organic matter in Wild 2 would have been captured during the Stardust mission by gas diffusion into the silica aerogel (Satoh et al. 1995). Volatiles captured as solid, frozen grains would have vaporized instantly upon impact. In fact, only three cometary volatile species, methylamine, ethylamine, and glycine have been identified in Stardust aerogel and on the Al foils surrounding the aerogel cells (Elsila et al. 2009). However, some less volatile, labile, cometary organics may have been successfully captured if intermixed with refractory organic matter. Any unprotected labile organic matter would most likely be broken down into more volatile products and lost during aerogel capture. In general, while volatile organic matter may dominate bulk carbonaceous matter in Wild 2, it is likely that any organic matter associated with captured cometary grains will be mostly composed of insoluble refractory material, with only a minor soluble component.

Three samples in this study contained silica aerogel associated with organic matter. Two of these are individual sections of a single particle (Particle 32) from Track 35 (Fig. 1A and 1B) and consist mainly of aerogel infiltrated with organic matter. A similar intermixing of aerogel and carbonaceous organic matter was inferred from infrared and Raman spectroscopy of other capture grains from Track 35 (Muñoz Caro et al. 2008). Not surprisingly, both samples from Track 35, Particle 32 have similar XANES spectra dominated by X-ray absorption at 287.5 eV due to aliphatic material, although this spectral feature may also be due to methyl groups intrinsic to the aerogel (Cody et al. 2008a; Sandford et al. 2010). Given the predominance of aerogel in the Track 35 samples observed directly by TEM, the XANES spectra can then be interpreted in two ways. In the first case, the XANES contribution from any cometary organic matter infiltrating the aerogel may be overprinted by photoabsorption from abundant methyl groups already present in the aerogel. In the second case, the functional group distribution of captured cometary organic matter may have been altered during capture, either through the formation of aliphatic bonds with nearby Si or O atoms or the selective separation and infiltration of less refractory, aliphatic, organic matter. As the abundance of carbon contamination within the aerogel is highly variable, up to several wt% C (Tsou et al. 2003; Sandford et al. 2006, 2010), the first interpretation cannot be eliminated. However, the second interpretation is more likely, as some type of alteration or fractionation would be expected for organic matter infiltrating several μm into the surrounding aerogel. Infrared spectroscopy of other capture tracks revealed halos of aliphatic organic matter infiltrating the aerogel surrounding the tracks by as much as 100 μm (Sandford et al. 2006; Bajt et al. 2009). Muñoz Caro et al. (2008) observed significant aliphatic organic matter mixed with aerogel extracted several mm from Track 35 grains, although this was interpreted as contamination intrinsic to the aerogel rather than infiltration of cometary organics. Diffusion of volatiles through high-porosity, ultralow density aerogel is rapid (Satoh et al. 1995) and aliphatic hydrocarbons have been observed to have high mass transport rates through catalyzing silica aerogels (Dunn et al. 2005). Larger, polyaromatic, macromolecular material would be less likely to infiltrate into compressed aerogel pore spaces than more labile aliphatic organic matter. Unfortunately, there is no method for determining whether the observed increase of aliphatic material in these samples was created during capture by interaction with silica aerogel or was already present as a component of the captured cometary organic matter.

Another aerogel-containing section, from Track 80, Particle 43 (Section A; Fig. 6A), contains both aerogel-free cometary organic matter and that which has

infiltrated the surrounding aerogel. However, XANES spectra show no chemical distinction between the infiltrating and free organic matter, which, unlike the previous aerogel-containing samples, does not contain abundant aliphatic organic matter (Fig. 7A). This difference may be due to the amount of aerogel in each sample. The Track 80 section only retains a total of about 2 μm^2 of surrounding aerogel in which the cometary organics have infiltrated, which may not be enough to significantly fractionate more aliphatic material from more polyaromatic material. In contrast, each of the Track 35 sections contains much more aerogel. Alternatively, the aerogel in which Track 80 is situated may be generally free of intrinsic carbon, while the aerogel around Track 35 may contain high levels of intrinsic carbon in the form of methyl and ethyl groups.

Epoxy-Soluble Organic Matter

During the PE of the Stardust returned samples, two epoxy-embedded samples were observed to contain an unexpected organic component present within the epoxy, apparently having originated from the embedded grains and migrated out into the surrounding epoxy (Cody et al. 2008a). XANES spectra of these extracted organics indicated the presence of an aliphatic material free of aromatic carbon (Sandford et al. 2006; Cody et al. 2008a). TEM and EELS observations in this study (Fig. 5) confirm these results and find that the extracted phase (which is a combination of epoxy and ~10% cometary organic matter) has a lower mass-density than the surrounding epoxy, resulting in brighter contrast in TEM images. Unfortunately, direct measurements of the composition and functional chemistry of this material are obfuscated by its solubility with epoxy. Cody et al. (2008a) estimate that each of these epoxy-soluble organics is extremely O-rich, with atomic O/C $\approx$ 0.6.

The observation of both labile, epoxy-soluble, organic matter and labile, aliphatic organic matter within aerogel (as described in the previous section) suggests that a significant soluble organic component exists on comet Wild 2 that was largely unaffected by aerogel capture, likely through shielding by surrounding mineral grains. Unfortunately, with current techniques, it is impossible to investigate whether this labile material contains the same diversity and complexity as soluble organic matter extracted from primitive chondrites (Schmitt-Kopplin et al. 2010).

Nitrogen-Rich Organic Matter

A significant observation from the PE of carbonaceous Stardust samples was the discovery of extremely N-rich organic matter in two samples (Sandford et al. 2006; Cody et al. 2008a). These two organic samples have a high atomic N/C = 0.24 but a lower O content (O/C $\approx$ 0.15) than most of the other Stardust organics. In this study, we report a third N-rich carbonaceous sample, from Track 80, Particle 43 (C2092,6,80,43,2 Section B; Fig. 6B). This third sample appears to be the most N rich of all the Stardust carbonaceous samples analyzed so far, with N/C = 0.36 estimated from XANES data and N/C = 0.20 measured by NanoSIMS. Unlike the other N-rich organics, it is also O-rich, with an atomic O/C = 0.43.

Subsequent TEM observations of two of these sections (C2115,24,22,1,5 from Track 22 and C2092,6,80,43,2 Section B from Track 80) provide evidence that this N-rich organic matter may be polymeric contamination. Unfortunately, the other N-rich, PE sample from Track 35, Particle 16 (C2054,0,35,16,4) was not available for further study. Both of the sections in the Track 22 sample (Fig. 4A) are clearly microtomed, indicating the material was most likely present in the grain plucked from the aerogel collector and embedded in sulfur. A possibility also exists for introduction of contaminants during particle embedding and although this procedure takes place in a clean environment and uses high-purity sulfur, evidence of smaller contaminant particles is found in early sections of Track 80, Particle 43 (C2092,6,80,43,1). Both sections have angular morphology and contain vesicular features. Their chemical functionality, derived from combined C-XANES and N-XANES, is aliphatic and dominated by amide ($CONH_x$) functional groups (Cody et al. 2008a), similar to amide polymers such as polyacrylamide and nylon. Wirick et al. (2009) also reported similar morphology and organic chemistry in adjacent ultramicrotome sections of this particle and they also suspected this material to likely be contamination. C-XANES and N-XANES of N-rich residues created by UV irradiation of mixtures of common interstellar organic molecules (Nuevo et al. 2011), thought to be a possible mechanism for the formation of cometary volatiles, also do not share spectral features with XANES spectra of the Track 22 sections. Furthermore, the smaller of the two sections contains several nanocrystals of anatase (TiO_2), which is both rare in primitive extraterrestrial materials and a common industrial contaminant. Subsequent ultramicrotome sections from this Track 22 particle consist of Fe-rich olivine, high-Ca pyroxene, and aluminosilicate glass in the absence of carbonaceous matter (Tomeoka et al. 2008), likely representing the true composition of the captured grain.

Section B from Track 80, Particle 43 (Fig. 6B) also contains many nanoscale metal-oxide crystallites, including Ti-oxide and several sulfide nanoparticles. The section also contains a sub-grain of turbostratic

carbon, which is commonly formed from heat-treatment or pyrolysis of organic or polymer precursors. The juxtaposition of high-melting-point oxides with low-melting-point sulfides, all trapped in a refractory organic matrix, is inconsistent with equilibrium (or even nonequilibrium) condensation in the early solar nebula. The functional group distribution of Section B is distinct from that of the Track 22 sections discussed above, but does share strikingly similar C- and N-XANES spectra with a ~2 μm organic, globular feature recovered from Stardust Track 2 (Fig. 7C and 7D; De Gregorio et al. 2010). The functionality of this Track 2 globule measured by XANES was observed to change dramatically after TEM analysis, indicating an extremely beam-sensitive material. However, as the original XANES spectrum of the Track 2 globule matched that of cyanoacrylate adhesive used in sample preparation of Stardust samples and the observed D enrichment in the globule matched the D enrichment that could be induced in cyanoacrylate exposed to a similar electron dose in the TEM, the Track 2 globule was interpreted as being most likely a cyanoacrylate contaminant introduced during sample preparation (De Gregorio et al. 2010). Unfortunately, XANES analysis was not performed on Section B prior to TEM analysis, so any chemical changes induced by the electron beam during TEM observation could not be quantified. However, the presence of abundant metal-oxides and turbostratic carbon, the lack of associated aerogel, and an organic functional chemistry similar to a probable contaminant grain from Track 2 suggests that Section B is also likely a contaminant.

It is still possible that the N-rich organic matter from Tracks 22 and 80 is authentic cometary material collected from Wild 2. The organic functionality of these samples is clearly distinct from the most likely aerogel and spacecraft contaminants analyzed by Sandford et al. (2010). In addition, the true variety of organic chemistry preserved within Wild 2 is still largely unknown, due to the currently small sample size of potentially cometary carbonaceous material in the Stardust collection. However, the presence of inorganic nanocrystals of unusual chemistry associated with these organic sections is difficult to interpret in a manner consistent with formation in the solar nebula.

A Possible Cometary Nanoglobule

Sample C2092,6,80,41,1 (Fig. 9) contains a single refractory carbonaceous grain with a highly aromatic organic functionality distinct from any observed during the PE samples (Sandford et al. 2006; Cody et al. 2008a) and all other organic samples in this study. However, its size and circular morphology and functional chemistry are reminiscent of an organic cometary globule reported by De Gregorio et al. (2010) in a different particle (Particle 43) from the same capture track. It is then possible that the Track 80, Particle 41 grain represents another aromatic cometary nanoglobule, although the nitrogen abundance in this sample is much lower than has been observed in isotopically anomalous nanoglobules in meteorites, IDPs, and Wild 2 (Garvie and Buseck 2004; Nakamura-Messenger et al. 2006; Messenger et al. 2008b; De Gregorio et al. 2010), precluding an accurate measurement of its $^{15}N/^{14}N$ ratio. In addition, most reported nanoglobules encompass a void space, which is absent in this particle. In any case, the sample represents the second reported example of predominantly aromatic cometary organic matter discovered in the Stardust collection.

Unaltered Cometary Organic Matter

Aside from the possible cometary nanoglobule described above, two additional samples contain organic matter with no apparent interaction with silica aerogel or the embedding media. These are the two adjacent sections of the terminal particle of Track 13 (FC9,0,13,1,5; Fig. 2). This particle is unambiguously extraterrestrial, as attested to by isotopic enrichments in both D (McKeegan et al. 2006) and ^{15}N (Table 3). XANES spectra of these sections indicate the presence of oxygenic carbonyl-type (C = O) functional groups (ketone, enol, and carboxyl groups), along with some aromatic C = C bonding (Cody et al. 2008a). Similar spectral features have been observed from carbonaceous matter in other Stardust samples (Matrajt et al. 2008; Wirick et al. 2009). These X-ray absorptions are also present in XANES spectra of IOM residues from primitive chondrite meteorites and carbonaceous matter in IDPs (Keller et al. 2004; Cody et al. 2008b), suggesting that the same organic precursors and physical processes that create IOM in meteorites and IDPs also generate at least some of the refractory organic matter preserved in comets. The XANES spectrum of Section A from Track 80, Particle 43 (C2092,6,80,43,2; Fig. 6A) also contains similar absorption peaks and although it also contains minor amounts of aerogel, it may be considered as composed of the same class of refractory organic matter.

The cometary organic matter in these sections does not show evidence of significant heating. XANES spectra of IOM from meteorites that have been heated on the parent body between 200 and 800 °C or flash heated up to 1400 °C exhibit a diagnostic absorption feature centered at 291.7 eV, recognized to be a 1s-σ* exciton associated with graphene domains (Cody et al. 2008b). The intensity of this excitonic peak increases with the parent body temperature and may be used as a geothermometer (Cody et al. 2008b). As the cometary

organic matter in this study is chemically similar to meteoritic IOM and shows no evidence of a 291.7 eV photoabsorption, this geothermometer estimates a maximum temperature experienced during aerogel capture of less than 150 °C. However, at the timescales of aerogel capture during the Stardust collection, the carbonization reactions may not proceed fast enough to approach equilibrium conditions. Under flash heating conditions, it is only possible to conclude that the Wild 2 organics in this study were not heated to greater than 1400 °C. However, the observation of surviving, labile, cometary organic matter associated with the more refractory material suggests that the actual temperature experienced during capture was much lower, approaching the low temperatures observed in experimental test shots into nonflight aerogel (Burchell et al. 2006; Spencer et al. 2009). Preservation of the Track 13 sample may have been aided by an intimate association with the silicate grain observed in adjacent ultramicrotome sections of this particle (Fig. 2C), which could have protected the organic matter from extreme temperature fluctuations during capture.

The identification of IOM-like cometary organic matter in the Stardust collection supports the hypothesis that IOM-like material was present in the early solar nebula, which could be incorporated into a variety of planetary materials. Disregarding the N- and O-rich Stardust samples, which may be altered organic matter or contaminants, the remaining Wild 2 organic samples contain highly variable abundances of N and O. Two samples, FC9,0,13,1,5 Section A and C2092,6,80,41,1, contain abundances in the range typical of meteoritic IOM, while the majority of the Wild 2 samples contain abundances similar to that observed in all but the most enriched IDPs (Fig. 10; Aléon et al. 2003; Cody et al. 2008a; Floss et al. 2010). This variability of N and O abundance in Wild 2 organics reflects the unequilibrated nature of the comet. Furthermore, all of the Wild 2 samples in this study contained terrestrial or slightly enriched $\delta^{15}N$ values, except for the extremely ^{15}N-rich organic globule from Track 80 (De Gregorio et al. 2010), indicating that the majority of the refractory organic matter preserved in the comet likely had a nebular origin (Fig. 10). Together, these observations imply that refractory organic matter in comets is generally more processed than that found in the most primitive chondritic porous IDPs (Ishii et al. 2008), although comets do contain some fraction of extremely primitive material, as indicated by large enrichments of ^{15}N in volatile CN comae (Schulz et al. 2008). While remaining at cold temperatures in the outer solar system, comets may still be a location for parent body processing of organic matter over billions of years (Fernández 2008; Prialnik et al. 2008). Although this processing would not be as efficient

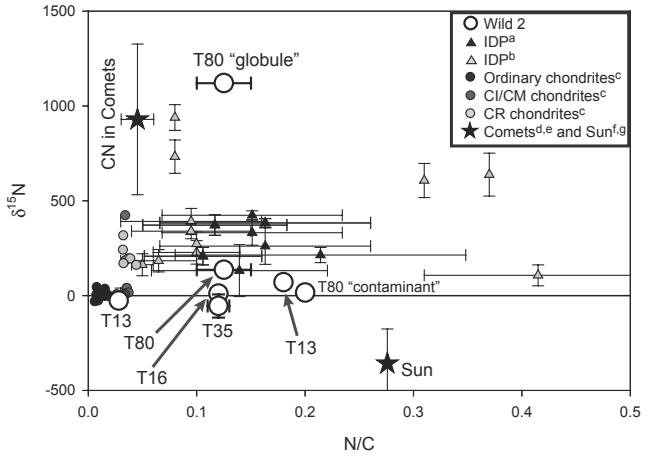

Fig. 10. Average atomic N/C and N isotopic compositions of Wild 2 samples, including a cometary organic globule previously reported in De Gregorio et al. (2010), compared with organic matter in primitive meteorites and IDPs. Labels refer to the aerogel track from which the sample was extracted. References: [a]Aléon et al. (2003), [b]Floss et al. (2010), [c]Alexander et al. (2007), [d]Huebner (2002), [e]Schulz et al. (2008), [f]Lodders (2003), [g]Marty et al. (2010).

as hydrothermal aqueous processing on asteroidal parent bodies, it could generate the more labile organic matter extracted from cometary grains during aerogel capture or epoxy-embedding. Alternatively, labile organic matter can be generated from volatile precursors by radiation processing of comet surfaces (Moore et al. 1983; Nuevo et al. 2011). Without extensive aqueous alteration on the parent body, these labile by-products will stay resident on the comet, without further significant degradation.

CONCLUSIONS

Transmission electron microscopy analyses of Stardust samples originally analyzed by STXM during the PE period indicate that the wide variety of organic functional groups observed (Sandford et al. 2006; Cody et al. 2008a) may be partly explained by a combination of molecular fractionation during aerogel capture and sample preparation. These include two of the three PE samples that showed evidence for abundant aliphatic hydrocarbons (C2054,0,35,32,8 and C2054,0,35,32,10), which both contained extensive areas of compressed silica aerogel in which cometary organic matter has filled pore spaces. The organic functional chemistry observed in the aerogel-rich sections may be due to selective extraction of labile aliphatic molecules during particle capture, leaving behind larger molecular weight, polyaromatic macromolecules that cannot easily fit in the compressed pore spaces. The two PE samples with extremely high O content (FC12,0,16,1,10 and the epoxy-soluble phase of C2054,0,35,16,4—not included in this

study) both resulted from dissolution of organic matter into the epoxy embedding medium. While it is likely that both of these types of organic matter may ultimately derive from cometary organics preserved in comet Wild 2, revealing important information about the more labile organic matter in the comet, there is still a possibility that these samples may be a result of contamination. For example, the aerogel into which Track 35 formed may have a local region of high intrinsic carbon contamination in the form of methyl and ethyl groups, resulting in an aliphatic overprint in XANES spectra and obscuring the true nature of the captured cometary organic matter. However unlikely, it is also possible that the O-rich epoxy-soluble organics were introduced during the procedure for particle extraction from the aerogel collector or embedding.

Two of the three extremely N-rich sections (C2115, 24,22,1,5 and C2092,6,80,43,2 Section B) were found to be most likely contaminants. Unfortunately, the third N-rich sample was not available for further study. Although the morphology and functional chemistry of these samples are distinct, both are composed of polymer-like material and contain nanoscale metal-oxide crystallites, which point to an industrial origin. It is not clear whether these samples, which were clearly ultramicrotomed, were present within the aerogel collector during the construction of the Stardust spacecraft or introduced later during sample preparation. However, it appears that N-rich organic matter with atomic N/C > 0.20 is less abundant in comet Wild 2 than previously thought.

Only three of the studied Stardust samples contain what appears to be relatively unaltered, refractory, cometary material. These are the two adjacent ultramicrotome sections from FC9,0,13,1,5, the partially aerogel-free section from C2092,6,80,43,2 Section A, and C2092,6,80,41,1. The first two of these samples have a functional chemistry similar to typical IOM found in meteorites and IDPs, as well as isotopic compositions demonstrating that they are cometary material. The latter sample is dominated by aromatic bonding, similar to that of a cometary organic globule reported by De Gregorio et al. (2010). In addition, it is likely that the organic matter present in the compressed aerogel sections from Track 35, Particle 32 (C2054,0,35,32,8 and C2054,0,35,32,10) is also IOM-like but modified by aliphatic bonding with the encompassing aerogel. These results suggest that the refractory organic matter present on comet Wild 2 is in actuality dominated by only two types of material—IOM-like organic matter and highly aromatic organic matter.

Acknowledgments—This work was funded by the Office of Naval Research, NASA Discovery Data Analysis and Origins of Solar Systems Program, and NASA Astrobiology Institute. This research was conducted while the primary author held a National Research Council Research Associateship at the U.S. Naval Research Laboratory. Use of the Advanced Light Source and the National Synchrotron Light Source was supported by the U.S. Department of Energy. Use of the Canadian Light Source was supported by the Natural Sciences and Engineering Research Council of Canada, the National Research Council Canada, the Canadian Institutes of Health Research, the Province of Saskatchewan, Western Economic Diversification Canada, and the University of Saskatchewan. The authors gratefully acknowledge the support of Thomas Zega and Nabil Bassim with the acquisition of STXM data.

Editorial Handling—Dr. Scott Sandford

REFERENCES

A'Hearn M. F. 2005. Deep impact: Excavating comet Tempel 1. *Science* 310:258–264.

Aléon J., Robert F., Chaussidon M., and Marty B. 2003. Nitrogen isotopic composition of macromolecular organic matter in interplanetary dust particles. *Geochimica et Cosmochimica Acta* 67:3773–3783.

Alexander C. M. O'D., Fogel M., Yabuta H., and Cody G. D. 2007. The origin and evolution of chondrites recorded in the elemental and isotopic compositions of their macromolecular organic matter. *Geochimica et Cosmochimica Acta* 71:4380–4403.

Apen E., Hitchcock A. P., and Gland J. L. 1993. Experimental studies of the core excitation of imidazole, 4, 5-dicyanoimidazole, and *s*-triazine. *Journal of Physical Chemistry* 97:6859–6866.

Bajt S., Sandford S. A., Flynn G. J., Matrajt G., Snead C. J., Westphal A. J., and Bradley J. P. 2009. Infrared spectroscopy of Wild 2 particle hypervelocity tracks in Stardust aerogel: Evidence for the presence of volatile organics in cometary dust. *Meteoritics & Planetary Science* 44:471–484.

Bassim N. D., De Gregorio B. T., Stroud R. M., and Fischione P. E. 2008. Study of FIB damage in carbonaceous materials using XANES. *Microscopy and Microanalysis* 14:1008–1009.

Berger E. L., Zega T. J., Keller L. P., and Lauretta D. S. 2011. Evidence for aqueous activity on comet 81P/Wild 2 from sulfide mineral assemblages in Stardust samples and CI chondrites. *Geochimica et Cosmochimica Acta* 75:3501–3513.

Brownlee D. E., Hörz F. P., Newburn R. L., Zolensky M. E., Duxbury T. C., Sandford S. A., Sekanina Z., Tsou P., Hanner M. S., Clark B. C., Green S. F., and Kissel J. 2004. Surface of young Jupiter family comet 81P/Wild 2: View from the Stardust spacecraft. *Science* 304:1764–1769.

Brownlee D. E., Tsou P., Aleon J., Alexander C. M. O'D., Araki T., Bajt S., Baratta G. A., Bastien R., Bland P., Bleuet P., Borg J., Bradley J. P., Brearley A., Brenker F., Brennan S., Bridges J. C., Browning N. D., Brucato J. R., Bullock E., Burchell M. J., Busemann H., Butterworth A., Chaussidon M., Cheuvront A., Chi M., Cintala M. J.,

Clark B. C., Clemett S. J., Cody G., Colangeli L., Cooper G., Cordier P., Daghlian C., Dai Z., D'Hendecourt L., Djouadi Z., Dominguez G., Duxbury T., Dworkin J. P., Ebel D. S., Economou T. E., Fakra S., Fairey S. A. J., Fallon S., Ferrini G., Ferroir T., Fleckenstein H., Floss C., Flynn G., Franchi I. A., Fries M., Gainsforth Z., Gallien J., Genge M., Gilles M. K., Gillet P., Gilmour J., Glavin D. P., Gounelle M., Grady M. M., Graham G. A., Grant P. G., Green S. F., Grossemy F., Grossman L., Grossman J. N., Guan Y., Hagiya K., Harvey R., Heck P., Herzog G. F., Hoppe P., Hörz F. P., Huth J., Hutcheon I. D., Ignatyev K., Ishii H. A., Ito M., Jacob D., Jacobsen C., Jacobsen S., Jones S., Joswiak D., Jurewicz A., Kearsley A. T., Keller L. P., Khodja H., Kilcoyne A. D., Kissel J., Krot A., Langenhorst F., Lanzirotti A., Le L., Leshin L. A., Leitner J., Lemelle L., Leroux H., Liu M., Luening K., Lyon I., MacPherson G., Marcus M. A., Marhas K., Marty B., Matrajt G., McKeegan K., Meibom A., Mennella V., Messenger K., Messenger S., Mikouchi T., Mostefaoui S., Nakamura T., Nakano T., Newville M., Nittler L. R., Ohnishi I., Ohsumi K., Okudaira K., Papanastassiou D. A., Palma R., Palumbo M. E., Pepin R. O., Perkins D., Perronnet M., Pianetta P., Rao W., Rietmeijer F. J. M., Robert F., Rost D., Rotundi A., Ryan R., Sandford S. A., Schwandt C. S., See T. H., Schlutter D., Sheffield-Parker J., Simionovici A., Simon S., Sitnitsky I., Snead C. J., Spencer M. K., Stadermann F. J., Steele A., Stephan T., Stroud R., Susini J., Sutton S. R., Suzuki Y., Taheri M., Taylor S., Teslich N., Tomeoka K., Tomioka N., Toppani A., Trigo-Rodríguez J. M., Troadec D., Tsuchiyama A., Tuzzolino A. J., Tyliszczak T., Uesugi K., Velbel M., Vellenga J., Vicenzi E., Vincze L., Warren J., Weber I., Weisberg M., Westphal A. J., Wirick S., Wooden D., Wopenka B., Wozniakiewicz P., Wright I., Yabuta H., Yano H., Young E. D., Zare R. N., Zega T., Ziegler K., Zimmerman L., Zinner E., and Zolensky M. 2006. Comet 81P/Wild 2 under a microscope. *Science* 314:1711–1716.

Burchell M. J., Mann J., Creighton J. A., Kearsley A. T., Graham G. A., and Franchi I. A. 2006. Identification of minerals and meteoritic materials via Raman techniques after capture in hypervelocity impacts on aerogel. *Meteoritics & Planetary Science* 41:217–232.

Burchell M. J., Foster N. J., Ormond-Prout J., Dupin D., and Armes S. P. 2009. Extent of thermal ablation suffered by model organic microparticles during aerogel capture at hypervelocities. *Meteoritics & Planetary Science* 44:1407–1419.

Busemann H., Young A. F., Alexander C. M. O'D., Hoppe P., Mukhopadhyay S., and Nittler L. R. 2006. Interstellar chemistry recorded in organic matter from primitive meteorites. *Science* 312:727–730.

Busemann H., Nguyen A. N., Cody G. D., Hoppe P., Kilcoyne A. D., Stroud R. M., Zega T. J., and Nittler L. R. 2009. Ultra-primitive interplanetary dust particles from the comet 26P/Grigg-Skjellerup dust stream collection. *Earth and Planetary Science Letters* 288:44–57.

Clemett S. J., Sandford S. A., Nakamura-Messenger K., Hörz F., and McKay D. S. 2010. Complex aromatic hydrocarbons in Stardust samples collected from comet 81P/Wild 2. *Meteoritics & Planetary Science* 45:701–722.

Cody G. D., Ade H., Alexander C. M. O'D., Araki T., Butterworth A., Fleckenstein H., Flynn G., Gilles M. K., Jacobsen C., Kilcoyne A. L. D., Messenger K., Sandford S. A., Tyliszczak T., Westphal A. J., Wirick S., and Yabuta H. 2008a. Quantitative organic and light-element analysis of comet 81P/Wild 2 particles using C-, N-, and O-μ-XANES. *Meteoritics & Planetary Science* 43:353–365.

Cody G. D., Alexander C. M. O'D., Yabuta H., Kilcoyne A. L. D., Araki T., Ade H., Dera P., Fogel M., Militzer B., and Mysen B. O. 2008b. Organic thermometry for chondritic parent bodies. *Earth and Planetary Science Letters* 272:446–455.

De Gregorio B. T., Stroud R. M., Nittler L. R., Alexander C. M. O'D., Kilcoyne A. D., and Zega T. J. 2010. Isotopic anomalies in organic nanoglobules from comet 81P/Wild 2: Comparison to Murchison nanoglobules and isotopic anomalies induced in terrestrial organics by electron irradiation. *Geochimica et Cosmochimica Acta* 74:4454–4470.

Dhez O., Ade H., and Urquhart S. G. 2003. Calibrated NEXAFS spectra of some common polymers. *Journal of Electron Spectroscopy and Related Phenomena* 128:85–96.

Dominguez G., Westphal A. J., Jones S. M., and Phillips M. L. 2004. Energy loss and impact cratering in aerogels: Theory and experiment. *Icarus* 172:613–624.

Dunn B. C., Cole P., Covington D., Webster M. C., Pugmire R. J., Ernst R. D., Eyring E. M., Shah N., and Huffman G. P. 2005. Silica aerogel supported catalysts for Fischer-Tropsch synthesis. *Applied Catalysis A: General* 278:233–238.

Elsila J. E., Glavin D. P., and Dworkin J. P. 2009. Cometary glycine detected in samples returned by Stardust. *Meteoritics & Planetary Science* 44:1323–1330.

Fernández J. 2008. Origin of comet nuclei and dynamics. *Space Science Reviews* 138:27–42.

Floss C., Stadermann F. J., Mertz A. F., and Bernatowicz T. J. 2010. A NanoSIMS and Auger Nanoprobe investigation of an isotopically primitive interplanetary dust particle from the 55P/Tempel-Tuttle targeted stratospheric dust collector. *Meteoritics & Planetary Science* 45:1889–1905.

Gallien J., Khodja H., Herzog G. F., Taylor S., Koepsell E., Daghlian C. P., Flynn G. J., Sitnitsky I., Lanzirotti A., Sutton S. R., and Keller L. P. 2008. Characterization of carbon- and nitrogen-rich particle fragments captured from comet 81P/Wild 2. *Meteoritics & Planetary Science* 43:335–351.

Garvie L. A. J. and Buseck P. R. 2004. Nanosized carbon-rich grains in carbonaceous chondrite meteorites. *Earth and Planetary Science Letters* 224:431–439.

Glavin D. P., Dworkin J. P., and Sandford S. A. 2008. Detection of cometary amines in samples returned by Stardust. *Meteoritics & Planetary Science* 43:399–413.

Gordon M. L., Cooper G., Morin C., Araki T., Turci C. C., Kaznacheyev K., and Hitchcock A. P. 2003. Inner-shell excitation spectroscopy of the peptide bond: Comparison of the C 1s, N 1s, and O 1s spectra of glycine, glycyl-glycine, and glycyl-glycyl-glycine. *Journal of Physical Chemistry A* 107:6144–6159.

Henke B. L., Gullikson E. M., and Davis J. C. 1993. X-Ray interactions: Photoabsorption, scattering, transmission, and reflection at E = 50-30,000 eV, Z = 1-92. *Atomic Data and Nuclear Data Tables* 54:181–342.

Hitchcock A. P. and Brion C. E. 1980. Inner-shell excitation of formaldehyde, acetaldehyde and acetone studied by electron impact. *Journal of Electron Spectroscopy and Related Phenomena* 19:231–250.

Huebner W. F. 2002. Composition of comets: Observations and models. *Earth, Moon, and Planets* 89:179–195.

Ishii I. and Hitchcock A. P. 1988. The oscillator strengths for C1*s* and O1*s* excitation of some saturated and unsaturated organic alcohols, acids and esters. *Journal of Electron Spectroscopy and Related Phenomena* 46:55–84.

Ishii H. A., Bradley J. P., Dai Z. R., Chi M., Kearsley A. T., Burchell M. J., Browning N. D., and Molster F. 2008. Comparison of comet 81P/Wild 2 dust with interplanetary dust from comets. *Science* 319:447–450.

Jacobsen C., Wirick S., Flynn G. J., and Zimba C. 2000. Soft X-ray spectroscopy from image sequences with sub-100 nm spatial resolution. *Journal of Microscopy* 197:173–184.

Kaznatcheev K., Karunakaran C., Lanke U., Urquhart S., Obst M., and Hitchcock A. 2007. Soft X-ray spectromicroscopy beamline at the CLS: Commissioning results. *Nuclear Instruments & Methods in Physics Research A* 582:96–99.

Keller L. P., Messenger S., Flynn G. J., Clemett S., Wirick S., and Jacobsen C. 2004. The nature of molecular cloud material in interplanetary dust. *Geochimica et Cosmochimica Acta* 68:2577–2589.

Keller L. P., Bajt S., Baratta G. A., Borg J., Bradley J. P., Brownlee D. E., Busemann H., Brucato J. R., Burchell M., Colangeli L., d'Hendecourt L., Djouadi Z., Ferrini G., Flynn G., Franchi I. A., Fries M., Grady M. M., Graham G. A., Grossemy F., Kearsley A., Matrajt G., Nakamura-Messenger K., Mennella V., Nittler L., Palumbo M. E., Stadermann F. J., Tsou P., Rotundi A., Sandford S. A., Snead C., Steele A., Wooden D., and Zolensky M. 2006. Infrared spectroscopy of comet 81P/Wild 2 samples returned by Stardust. *Science* 314:1728–1731.

Kikuma J., Warwick T., Shin H.-J., Zhang J., and Tonner B. P. 1998. Chemical state analysis of heat-treated polyacrylonitrile fiber using soft X-ray spectromicroscopy. *Journal of Electron Spectroscopy and Related Phenomena* 94:271–278.

Kilcoyne A. L., Tyliszczak T., Steele W. F., Fakra S., Hitchcock P., Franck K., Anderson E., Harteneck B., Rightor E. G., Mitchell G. E., Hitchcock A. P., Yang L., Warwick T., and Ade H. 2003. Interferometer-controlled scanning transmission X-ray microscopes at the Advanced Light Source. *Journal of Synchrotron Radiation* 10:125–136.

Kissel J., Krueger F. R., Silen J., and Clark B. C. 2004. The cometary and interstellar dust analyzer at comet 81P/Wild 2. *Science* 304:1774–1776.

Leinweber P., Kruse J., Walley F. L., Gillespie A., Eckhardt K., Blyth R. I. R., and Regier T. 2007. Nitrogen *K*-edge XANES—An overview of reference compounds used to identify "unknown" organic nitrogen in environmental samples. *Journal of Synchrotron Radiation* 14:500–511.

Lerotic M., Jacobsen C., Schäfer T., and Vogt S. 2004. Cluster analysis of soft X-ray spectromicroscopy data. *Ultramicroscopy* 100:35–57.

Leroux H., Rietmeijer F. J. M., Velbel M. A., Brearley A. J., Jacob D., Langenhorst F., Bridges J. C., Zega T. J., Stroud R. M., Cordier P., Harvey R. P., Lee M., Gounelle M., and Zolensky M. E. 2008. A TEM study of thermally modified comet 81P/Wild 2 dust particles by interactions with the aerogel matrix during the Stardust capture process. *Meteoritics & Planetary Science* 43:97–120.

Leroux H., Roskosz M., and Jacob D. 2009. Oxidation state of iron and extensive redistribution of sulfur in thermally modified Stardust particles. *Geochimica et Cosmochimica Acta* 73:767–777.

Lodders K. 2003. Solar system abundances and condensation temperatures of the elements. *The Astrophysical Journal* 591:1220–1247.

Marcus M. A., Fakra S., Westphal A. J., Snead C. J., Keller L. P., Kearsley A., and Burchell M. J. 2008. Smelting of Fe-bearing glass during hypervelocity capture in aerogel. *Meteoritics & Planetary Science* 43:87–96.

Marty B., Palma R. L., Pepin R. O., Zimmermann L., Schlutter D. J., Burnard P. G., Westphal A. J., Snead C. J., Bajt S., Becker R. H., and Simones J. E. 2008. Helium and neon abundances and compositions in cometary matter. *Science* 319:75–78.

Marty B., Zimmermann L., Burnard P. G., Wieler R., Heber V. S., Burnett D. L., Wiens R. C., and Bochsler P. 2010. Nitrogen isotopes in the recent solar wind from the analysis of Genesis targets: Evidence for large scale isotope heterogeneity in the early solar system. *Geochimica et Cosmochimica Acta* 74:340–355.

Matrajt G., Ito M., Wirick S., Messenger S., Brownlee D. E., Joswiak D., Flynn G., Sandford S., Snead C., and Westphal A. 2008. Carbon investigation of two Stardust particles: A TEM, NanoSIMS, and XANES study. *Meteoritics & Planetary Science* 43:315–334.

McKeegan K. D., Aleon J., Bradley J., Brownlee D. E., Busemann H., Butterworth A., Chaussidon M., Fallon S., Floss C., Gilmour J., Gounelle M., Graham G., Guan Y., Heck P. R., Hoppe P., Hutcheon I. D., Huth J., Ishii H. A., Ito M., Jacobsen S. B., Kearsley A., Leshin L. A., Liu M., Lyon I., Marhas K., Marty B., Matrajt G., Meibom A., Messenger S., Mostefaoui S., Mukhopadhyay S., Nakamura-Messenger K., Nittler L., Palma R., Pepin R. O., Papanastassiou D. A., Robert F., Schlutter D., Snead C. J., Stadermann F. J., Stroud R., Tsou P., Westphal A., Young E. D., Ziegler K., Zimmermann L., and Zinner E. 2006. Isotopic compositions of cometary matter returned by Stardust. *Science* 314:1724–1728.

Messenger S. 2000. Identification of molecular-cloud material in interplanetary dust particles. *Nature* 404:968–971.

Messenger S., Ito M., Joswiak D. J., Keller L. P., Stroud R. M., Nakamura-Messenger K., Matrajt G., and Brownlee D. E. 2008a. Oxygen isotopic compositions of Wild 2 silicates. *Meteoritics and Planetary Science* 43:A97.

Messenger S., Nakamura-Messenger K., and Keller L. P. 2008b. ^{15}N-rich organic globules in a cluster IDP and the Bells CM2 chondrite (abstract #2391). 39th Lunar and Planetary Science Conference. CD-ROM.

Moore M. H., Donn B., Khanna R., and A'Hearn M. F. 1983. Studies of proton-irradiated cometary-type ice mixtures. *Icarus* 54:388–405.

Muñoz Caro G. M., Dartois E., and Nakamura-Messenger K. 2008. Characterization of the carbon component in cometary Stardust samples by means of infrared and Raman spectroscopy. *Astronomy & Astrophysics* 485:743–751.

Nakamura T., Noguchi T., Tsuchiyama A., Ushikubo T., Kita N. T., Valley J. W., Zolensky M. E., Kakazu Y., Sakamoto K., Mashio E., Uesugi K., and Nakano T. 2008. Chondrulelike objects in short-period comet 81P/Wild 2. *Science* 321:1664–1667.

Nakamura-Messenger K., Messenger S., Keller L. P., Clemett S. J., and Zolensky M. E. 2006. Organic globules in the Tagish Lake meteorite: Remnants of the protosolar disk. *Science* 314:1439–1442.

Noguchi T., Nakamura T., Okudaira K., Yano H., Sugita S., and Burchell M. J. 2007. Thermal alteration of hydrated minerals during hypervelocity capture to silica aerogel at the flyby speed of Stardust. *Meteoritics & Planetary Science* 42:357–372.

Nuevo M., Milam S. N., Sandford S. A., De Gregorio B. T., Cody G. D., and Kilcoyne A. L. D. 2011. XANES analysis of organic residues produced from the UV irradiation of astrophysical ice analogs. *Advances in Space Research*, doi:10.1016/j.asr.2011.05.020.

Phalippou J., Despetis F., Calas S., Faivre A., Dieudonné P., Sempéré R., and Woignier T. 2004. Comparison between sintered and compressed aerogels. *Optical Materials* 26:167–172.

Prialnik D., Sarid G., Rosenberg E., and Merk R. 2008. Thermal and chemical evolution of comet nuclei and Kuiper Belt objects. *Space Science Reviews* 138:147–164.

Rietmeijer F. J. M., Nakamura T., Tsuchiyama A., Uesugi K., Nakano T., and Leroux H. 2008. Origin and formation of iron silicide phases in the aerogel of the Stardust mission. *Meteoritics & Planetary Science* 43:121–134.

Rightor E. G., Hitchcock A. P., Ade H., Leapman R. D., Urquhart S. G., Smith A. P., Mitchell G., Fischer D., Shin H. J., and Warwick T. 1997. Spectromicroscopy of poly(ethylene terephthalate): Comparison of spectra and radiation damage rates in X-ray absorption and electron energy loss. *Journal of Physical Chemistry B* 101:1950–1960.

Rotundi A., Baratta G. A., Borg J., Brucato J. R., Busemann H., Colangeli L., d'Hendecourt L., Djouadi Z., Ferrini G., Franchi I. A., Fries M., Grossemy F., Keller L. P., Mennella V., Nakamura K., Nittler L. R., Palumbo M. E., Sandford S. A., Steele A., and Wopenka B. 2008. Combined micro-Raman, micro-infrared, and field emission scanning electron microscope analyses of comet 81P/Wild 2 particles collected by Stardust. *Meteoritics & Planetary Science* 43:367–397.

Sandford S. A., Aleon J., Alexander C. M. O'D., Araki T., Bajt S., Baratta G. A., Borg J., Bradley J. P., Brownlee D. E., Brucato J. R., Burchell M. J., Busemann H., Butterworth A., Clemett S. J., Cody G., Colangeli L., Cooper G., D'Hendecourt L., Djouadi Z., Dworkin J. P., Ferrini G., Fleckenstein H., Flynn G. J., Franchi I. A., Fries M., Gilles M. K., Glavin D. P., Gounelle M., Grossemy F., Jacobsen C., Keller L. P., Kilcoyne A. L. D., Leitner J., Matrajt G., Meibom A., Mennella V., Mostefaoui S., Nittler L. R., Palumbo M. E., Papanastassiou D. A., Robert F., Rotundi A., Snead C. J., Spencer M. K., Stadermann F. J., Steele A., Stephan T., Tsou P., Tyliszczak T., Westphal A. J., Wirick S., Wopenka B., Yabuta H., Zare R. N., and Zolensky M. E. 2006. Organics captured from comet 81P/Wild 2 by the Stardust spacecraft. *Science* 314:1720–1724.

Sandford S. A., Bajt S., Clemett S. J., Cody G. D., Cooper G., De Gregorio B. T., De Vera V., Dworkin J. P., Elsila J. E., Flynn G. J., Glavin D. P., Lanzirotti A., Limero T., Martin M. P., Snead C. J., Spencer M. K., Stephan T., Westphal A., Wirick S., Zare R. N., and Zolensky M. E. 2010. Assessment and control of organic and other contaminants associated with the Stardust sample return from comet 81P/Wild 2. *Meteoritics & Planetary Science* 45:406–433.

Satoh S., Matsuyama I., and Susa K. 1995. Diffusion of gases in porous silica gel. *Journal of Non-Crystalline Solids* 190:206–211.

Schmitt-Kopplin P., Gabelica Z., Gougeon R. D., Fekete A., Kanawati B., Harir M., Gebefuegi I., Eckel G., and Hertkorn N. 2010. High molecular diversity of extraterrestrial organic matter in Murchison meteorite revealed 40 years after its fall. *Proceedings of the National Academy of Sciences of the United States of America* 107:2763–2768.

Schulz R., Jehin E., Manfroid J., Hutsemékers D., Arpigny C., Cochran A., Zucconi J., and Stüwe J. 2008. Isotopic abundance in the CN coma of comets: Ten years of measurements. *Planetary and Space Science* 56:1713–1718.

Shard A. G., Whittle J. D., Beck A. J., Brookes P. N., Bullett N. A., Talib R. A., Mistry A., Barton D., and McArthur S. L. 2004. A NEXAFS examination of unsaturation in plasma polymers of allylamine and propylamine. *Journal of Physical Chemistry B* 108:12472–12480.

Spencer M. K., Clemett S. J., Sandford S. A., McKay D. S., and Zare R. N. 2009. Organic compound alteration during hypervelocity collection of carbonaceous materials in aerogel. *Meteoritics & Planetary Science* 44:15–24.

Stadermann F. J., Hoppe P., Floss C., Heck P. R., Hörz F., Huth J., Kearsley A. T., Leitner J., Marhas K. K., Mckeegan K. D., and Stephan T. 2008. Stardust in Stardust—The C, N, and O isotopic compositions of Wild 2 cometary matter in Al foil impacts. *Meteoritics & Planetary Science* 43:299–313.

Stern A. S. 2003. The evolution of comets in the Oort cloud and Kuiper belt. *Nature* 424:639–642.

Stodolna J., Jacob D., and Leroux H. 2009. A TEM study of four particles extracted from the Stardust track 80. *Meteoritics & Planetary Science* 44:1511–1518.

Stöhr J. 1992. *NEXAFS Spectroscopy*. Berlin: Springer. 403 p.

Stroud R. M., Long J. W., Pietron J. J., and Rolison D. R. 2004. A practical guide to transmission electron microscopy of aerogels. *Journal of Non-Crystalline Solids* 350:277–284.

Tomeoka K., Tomioka N., and Ohnishi I. 2008. Silicate minerals and Si-O glass in comet Wild 2 samples: Transmission electron microscopy. *Meteoritics & Planetary Science* 43:273–284.

Tsou P., Brownlee D. E., Sandford S. A., Hörz F., and Zolensky M. E. 2003. Wild 2 and interstellar sample collection and Earth return. *Journal of Geophysical Research* 108:8113.

Urquhart S. G. and Ade H. 2002. Trends in the carbonyl core (C 1S, O 1S) $\rightarrow$ $\pi^*_{C=O}$ transition in the near-edge X-ray absorption fine structure spectra of organic molecules. *Journal of Physical Chemistry B* 106:8531–8538.

Urquhart S. G., Hitchcock A. P., Priester R. D., and Rightor E. G. 1995. Analysis of polyurethanes using core excitation spectroscopy. Part II: Inner shell spectra of ether, urea and carbamate model compounds. *Journal of Polymer Science B* 33:1603–1620.

Westphal A. J., Fakra S. C., Gainsforth Z., Marcus M. A., Ogliore R. C., and Butterworth A. L. 2009. Mixing fraction of inner solar system material in comet 81P/Wild 2. *The Astrophysical Journal* 694:18–28.

Winn B., Ade H., Buckley C., Feser M., Howells M., Hulbert S., Jacobsen C., Kaznacheyev K., Kirz J., Osanna A., Maser J., McNulty I., Miao J., Oversluizen T., Spector S., Sullivan B., Wang Y., Wirick S., and Zhang H. 2000. Illumination for coherent soft X-ray applications: The new X1A beamline at the NSLS. *Journal of Synchrotron Radiation* 7:395–404.

Wirick S., Flynn G. J., Keller L. P., Nakamura-Messenger K., Peltzer C., Jacobsen C., Sandford S., and Zolensky M. 2009. Organic matter from comet 81P/Wild 2, IDPs, and

carbonaceous meteorites; similarities and differences. *Meteoritics & Planetary Science* 44:1611–1626.

Wozniakiewicz P. J., Ishii H. A., Kearsley A. T., Burchell M. J., Bradley J. P., Teslich N., and Cole M. J. 2010. Survivability of cometary phyllosilicates in Stardust collections and implications for the nature of comets (abstract #2357). 41st Lunar and Planetary Science Conference. CD-ROM.

Zhou D., Metzler R. A., Tyliszczak T., Guo J., Abrecht M., Coppersmith S. N., and Gilbert P. U. P. A. 2008. Assignment of polarization-dependent peaks in carbon K-edge spectra from biogenic and geologic aragonite. *The Journal of Physical Chemistry B* 112:13128–13135.

Zolensky M. E., Zega T. J., Yano H., Wirick S., Westphal A. J., Weisberg M. K., Weber I., Warren J. L., Velbel M. A., Tsuchiyama A., Tsou P., Toppani A., Tomioka N., Tomeoka K., Teslich N., Taheri M., Susini J., Stroud R., Stephan T., Stadermann F. J., Snead C. J., Simon S. B., Simionovici A., See T. H., Robert F., Rietmeijer F. J. M., Rao W., Perronnet M. C., Papanastassiou D. A., Okudaira K., Ohsumi K., Ohnishi I., Nakamura-Messenger K., Nakamura T., Mostefaoui S., Mikouchi T., Meibom A., Matrajt G., Marcus M. A., Leroux H., Lemelle L., Le L., Lanzirotti A., Langenhorst F., Krot A. N., Keller L. P., Kearsley A. T., Joswiak D., Jacob D., Ishii H., Harvey R., Hagiya K., Grossman L., Grossman J. N., Graham G. A., Gounelle M., Gillet P., Genge M. J., Flynn G., Ferroir T., Fallon S., Ebel D. S., Dai Z. R., Cordier P., Clark B., Chi M., Butterworth A. L., Brownlee D. E., Bridges J. C., Brennan S., Brearley A., Bradley J. P., Bleuet P., Bland P. A., and Bastien R. 2006. Mineralogy and petrology of comet 81P/Wild 2 nucleus samples. *Science* 314:1735–1739.